Combining Hypoxia-Activated Prodrugs and Radiotherapy *in silico*: Impact of Treatment Scheduling and the Intra-Tumoural Oxygen Landscape

Sara Hamis[1,2], Mohammad Kohandel[3], Ludwig J Dubois[4], Ala Yaromina[4] Philippe Lambin[4] Gibin G Powathil[2]

[1] School of Mathematics and Statistics, University of St Andrews, St Andrews KY16 9SS, Scotland.
[2] Department of Mathematics, College of Science, Swansea University, Swansea, SA1 8EN, United Kingdom.
[3] Department of Applied Mathematics, University of Waterloo, Waterloo, Canada.
[4] The M-Lab, Department of Precision Medicine, GROW – School for Oncology and Developmental Biology, Maastricht University, Maastricht, The Netherlands.

Abstract

Hypoxia-activated prodrugs (HAPs) present a conceptually elegant approach to not only overcome, but better yet, exploit intra-tumoural hypoxia. Despite being successful *in vitro* and *in vivo*, HAPs are yet to achieve successful results in clinical settings. It has been hypothesised that this lack of clinical success can, in part, be explained by the insufficiently stringent clinical screening selection of determining which tumours are suitable for HAP treatments [1].

We here demonstrate that both the intra-tumoural oxygen landscape and treatment scheduling of HAP-radiation combination therapies influence treatment responses *in silico*. Our *in silico* framework is based on an on-lattice, hybrid, multiscale cellular automaton spanning three spatial dimensions. The mathematical model for tumour spheroid growth is parameterised by multicellular tumour spheroid (MCTS) data.

Keywords

Hypoxia-Activated Prodrugs, Ionising Radiation, Agent-Based Mathematical Model, Personalised Oncology

1 Introduction

Oxygen concentrations vary across solid tumours and, although tumours present with high diversity across patients [2], hypoxic regions are prevalent tumour features [3, 4, 5, 6, 7, 8, 9, 10, 11] commonly provoked by inadequate oxygen supply and high tumour growth rates [12]. Hypoxia significantly impacts tumour dynamics, treatment responses and, by extension, clinical outcomes [13, 6, 9]. Hypoxia may alter cellular expressions of genomes, proteins and epigenetic traits [12], and such hypoxia-induced alterations may cause hypoxic cancer cells to be more resistant to apoptosis [14]. Hypoxia may also alter the metabolism of cells [14], promote angiogenesis by activating associated genes [15] and upregulate efflux systems [16]. Thus hypoxia both protects and progresses solid tumours [14, 13]. Accordingly, severe tumour hypoxia is associated with tumours that are difficult to treat and, by extension, poor prognoses for patients [12, 7]. It is well established that hypoxic regions in solid tumours express reduced sensitivity to radiotherapy and a plethora of chemotherapeutic drugs [12, 15, 17, 14, 6, 7, 18, 8, 9, 19, 11]. Hypoxic cancer cells in a solid tumour are naturally located far away from active oxygen sources, i.e. blood vessels [7], and therefore drug molecules that are of large size or tightly bound to cell components may not reach hypoxic tumour cells at all [15]. Moreover, genes associated with chemo-resistance may be upregulated by hypoxia [1]. Hypoxia is also regarded to be one of the main factors contributing to radiotherapy failure [15]. Radiation-induced DNA damage, especially in the form of double strand breaks, is more easily self-repaired by the cell under hypoxic conditions [20].

Due to their severe impact on conventional anticancer therapies, such as chemotherapy and radiotherapy, hypoxic cancer cells, and their central mediators [12], have for the last decades been considered to be important treatment-targets [15, 2]. In treatment scenarios in which rapid tumour re-oxygenation does not occur, hypoxic tumour regions can, instead, be more directly targeted. Multiple ways to handle tumour hypoxia have been explored. One approach to combat intratumoural hypoxia is to increase the tumour oxygenation as part of a neoadjuvant treatment [1]. A second approach to overcome hypoxia is to selectively target hypoxic cancer cells only for treatment-sensitising or eradication [4]. A third and conceptually elegant approach to not only overcome, but better yet, exploit intratumoural hypoxia is realised by hypoxia-activated prodrugs (HAPs) [15]. HAPs are bioreductive prodrugs that reduce, and thus convert, into cytotoxic agents upon reaching hypoxic (tumour) regions [14, 19]. Theoretically, they act as Trojan horses, ideally being essentially harmless until they are converted into warheads in target regions, i.e. hypoxic (tumour) cells. The tumour-targeting ability of HAPs is based on the premise that oxygen concentrations in hypoxic tumour regions reach exceptionally low levels, and that such low oxygen levels are much more prevalent in tumours, than in the body tissue that locally surrounds the tumours [14]. Indeed physoxia, that is the term commonly used to describe oxygen levels found in several types of normal tissue, ranges between 10 and 80 mmHg, and a cancer cell is commonly classified as hypoxic if it has a partial pressure of oxygen (pO_2) value of 10 mmHg or less [5]. Solid tumours commonly display regions that are even more hypoxic, where pO_2 values may drop below 5 mmHg [5]. Consequently, HAPs theoretically constitute a means to effectively target hypoxic tumour cells. This also means that toxic drug effects can be localised to tumours, and that the remaining host system can in great part be spared from harmful toxicity causing unwanted side effects.

HAPs transform into activated drugs (AHAPs) via reductive metabolism [15, 3] in sufficiently hypoxic environments, and the AHAPs can achieve cytotoxic effects in cells [21]. Freely available molecular oxygen may inhibit this bioreduction, and thus HAPs remain (for the most part) more intact, and by extension less toxic, in well-oxygenated environments [14]. Once activated, certain AHAPs may diffuse into their local surroundings. Thus, via bystander effects, for certain HAP drugs, AHAPs may infer damage to cells in which the HAP-to-AHAP bioreduction did not occur. However, a few recent studies dispute the impact of these bystander effects on the overall treatment outcome [22]. In the mathematical model described in this study, the dispersion of HAPs and AHAPs obey mechanistic diffusion equations, and the reach of AHAPs can easily be modified by altering coefficients in the AHAP diffusion equation. Thus the influence of bystander effects on the treatment outcome is allowed to range from *negligable* to *highly influential* in our mathematical model.

Multiple HAPs have been evaluated for their clinical potential, both as monotherapies and as part of combination therapies [12, 8]. Class I HAPs are activated in moderately hypoxic environments whilst Class II HAPs require more severe hypoxia to undergo the HAP to AHAP bioreduction [23]. One such Class II HAP is evofosfamide, or TH-302, which has been tested in clinical Phase I-III trials [12, 1]. TH-302 bioreduces to its activated form, bromo-isophosphoramide mustard (Br-IPM), in hypoxic tumour regions, and Br-IPM is a DNA-crosslinking agent [22]. Multiple *in vitro* and *in vivo* studies have validated this drug's preclincal success and, by extension, its clinical feasibility [13, 24, 25, 26, 6, 7, 18, 27, 9, 21, 10, 28]. Multimodality treatment strategies combining HAPs, particularly Class II HAPs, with ionising radiation (IR) may be particularly promising [29, 8, 9, 27, 28] as the two therapies conceptually complement each other: HAPs target hypoxic tumour regions whilst radiotherapy is most effective against well oxygenated tumour regions. Thus, in principal, HAP-IR combination treatments have the ability to produce multifaceted attacks on tumours.

Despite HAPs being conceptually promising and successful in laboratories, this success has not yet been mirrored in clinical trials [12, 2, 1]. It is hypothesised that this unsuccessful *Bench-to-Bedside* translation is partly due to an insufficiently stringent clinical screening practice of selecting tumours that are suitable for HAP treatments [1]. It is likely that some of the tumours enrolled in clinical trials have been insufficiently hypoxic to benefit from treatment plans involving HAPs [2]. To investigate this hypothesis, we here propose a mathematical modelling angle to simulate how spatio-temporal tumour features may impact HAP efficacy and how scheduling influences the outcome of multimodality HAP-IR treatments.

Today, mathematical modelling constitutes an indispensable complement to traditional cancer research. Models provide an opportunity to study biological phenomena *in silico* that may not be empirically observable and, moreover, *in silico* experiments are fast and cheap to run, easy to reproduce and not directly associated with any ethical concerns. Previous mathematical studies have already contributed to the overall understanding of HAPs, quantified key mechanisms associated to them and illustrated their clinical feasibility. Foehrenbacher *et al.* [30] have deployed a Green's function method, in customised form, and pharmacokinetic/pharmacodynamic

(PK/PD) modelling to quantify anticancer bystander effects elicited by the HAP PR-104 in a simulated, three-dimensional tumour comprising a microvascular network. Another concurrent article used similar mathematical concepts to compare Class I HAPs to Class II HAPs and, furthermore, to determine optimal properties for Class II HAPs [23]. Lindsay *et al.* [31] developed a stochastic model to study monotherapies and combination therapies involving HAPs, specifically TH-302, and erlotinib. Amongst other findings, they concluded that a combination therapy of the two drugs impedes the uprising of drug resistance. Since HAPs bioreduce to activated form under hypoxic conditions it follows that AHAP activity increases with intratumoural hypoxia. Accordingly, a previous study by Wojtkowiak *et al.* [32] conceptually validated the strategy of amplifying TH-302 activity by deliberately exacerbating intratumoural hypoxia using exogenous pyruvate. Their study combined mathematical modelling with metabolic profiling and EPR (electron paramagnetic resonance) imaging. HAP dynamics were modelled using reaction-diffusion/convection equations coupled with fluid-structure interactions. In line with these previous mathematical studies, the aim of this *in silico* study is to contribute HAP-related insights gained by mathematical modelling, according to a *Blackboard-to-Bedside* [33] approach.

In clinical settings, the intratumoural oxygenation status can be assessed in multiple ways. By inserting oxygen electrodes into tumours, pO_2 values can directly be measured, but this measuring technique is invasive and does not distinguish between hypoxic and necrotic tumour regions [1]. Alternatively, less invasive imaging techniques, such as positron emission (PET-scans) and oxygen-enhanced magnetic resonance (MRIs), can be used to evaluate oxygen levels in tumours [12, 1]. Moreover, there now exist several hypoxia gene expression signatures that may be used to characterise hypoxia-related tumour features, and some of these signatures have been conferred with poor clinical prognoses [1]. Avoiding a tumour biopsy, by measuring hypoxia secreted markers in the blood, would, furthermore, constitute a more expeditious way to assess tumour hypoxia [1]. Without further discussing the advantages and disadvantages of various hypoxia assessment methods, the above discussion illustrates that it is, indeed, feasible to invoke stricter selection regimes when deciding whether or not to pair tumours with HAP treatments in clinical trials [1]. A recent publication, by Spiegelberg *et al.* [1], claims that the (lack of) clinical progress with HAP-treatments can, in great part, be attributed to the omission of hypoxia-based patient selection in phase III trials. In this study, we demonstrate that the efficacy of HAP monotherapies and HAP-IR combination therapies *in silico* is, indeed, highly dependent on tumour-specific oxygen features.

2 Model

An on-lattice, hybrid, multiscale cellular automaton (CA) is here used to model solid tumours subjected to HAP and IR monotherapies, as well as HAP-IR combination therapies. Tumour growth and HAP responses are parameterised by published data from an *in vitro* study performed by Voissiere *et al.* [34], in which multicellular tumour spheroids (MCTSs) where grown and exposed to HAPs. Specifically, we use their data for human chondrosarcoma HEMC-SS cells exposed to the hypoxia activated prodrug TH-302. Our mathematical model is thereafter extended to simulate *in vivo* drug dynamics in order to investigate scheduling aspects of HAP-IR

combination therapies. The parameters used in this paper can be modified in order to simulate specific cell-lines and drugs, and model rules can be altered in order to simulate both *in vitro* and *in vivo* cancer cell populations, MCTSs or tumours. Thus, with the availability of appropriate data, various tumour scenarios and treatment schedules and doses can be investigated *in silico*. Hence the mathematical model presented here constitutes a valuable and versatile complement to both *in vitro* and *in vivo* experiments. The model used in this study is an extension of a previous, well-established model presented by Powathil *et al.* [35]. All parameters used in the model are motivated from experiments and literature, as described throughout this section, and are summarised in Section 2.7, Table 1.

2.1 Mathematical Framework: A Cellular Automaton (CA)

The CA used in this model allows for spatio-temporal dynamics and intratumoural heterogeneity including variations in cell-cycle progression, oxygen levels, drug concentrations and treatment responses amongst cancer cells [35, 36, 33, 37]. The model is multiscale and integrates both intracellular and extracellular regulations. *In vitro* experiments have demonstrated that MCTSs are more HAP-sensitive than are monolayers. This increase in sensitivity has been attributed to the microenvironment correlated to multilayer cultures [18]. Aspiring to achieve an *in silico* model that is as clinically relevant as possible, we here let the CA lattice extend in three spatial dimensions. The lattice is specifically a square lattice containing 100^3 lattice points, simulating a physical environment of $(2\text{mm})^3$. Thus each voxel in the lattice spans a volume of $(20\mu\text{m})^3$ and each lattice point may be occupied by either one cancer cell or extracellular matrix. These dimensions agree with previous mathematical studies [35], and cell population density in the MCTSs that are used to calibrate the model [34]. The time step used to model the temporal progression of the CA is $\Delta t = 10^{-4}$ hours, by appropriate non-dimensionalisation of oxygen dynamics [35].

2.2 Cell-Cycle Progression

On an intracellular scale, sub-cellular mechanisms are modelled individually for each cell in order to allow for variations amongst cancer cells. Cell-cycle progression is one such intracellular process, it is governed by an intrinsic cell-cycle clock attributed to each individual cell. In order to account for cell-cycle asynchronicity amongst cells, each cell i is assigned an individual, stochastic doubling-time τ_i which corresponds to the time it takes for a cell to complete one cell-cycle, and double by producing a daughter cell, in well-oxygenated conditions. Here, τ_i is picked from a normal distribution [36] with a mean value μ and a standard deviation σ, which are picked to match cell population growth-rates reported from Voissiere *et al.* [34]. as demonstrated in Figure 1.

Each cell in the model follows a cell-cycle typical to that of eukaryotic cells. In particular, a cell is defined to be in the gap 1 (G1), synthesis (S), gap 2 (G2) or mitosis (M) phase of the cell-cycle. As sensitivity to radiotherapy is cell-cycle dependent [20], it is important to track cell-cycle phase progression in the model. Each cell that is placed on the lattice commences its first cell-cycle in the G1 phase. Under well-oxygenated conditions, the fraction of time spent in

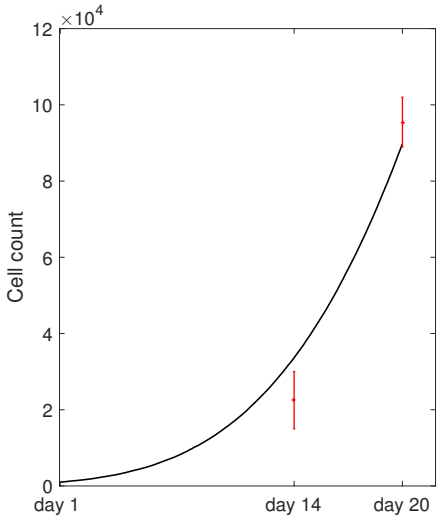

Figure 1: Cell count over time for tumour spheroids. The *in silico* data is based on 10 simulations runs, the mean (black line) is shown. *In vitro* data (red error bars) are gathered from Voissiere *et al.* [34].

each of the four distinct cell-cycle phases are Θ_{G1}, Θ_S, Θ_{G2} and Θ_M for the cell-cycle phases G1, S, G2, M respectively, where the Θ-fractions sum up to one so that

$$\Theta_{G1} + \Theta_S + \Theta_{G2} + \Theta_M = 1. \tag{1}$$

The four theta values are picked from literature in order to match typical cell cycle phase lengths of rapidly cycling human cells with a doubling time of roughly 24 hours [38]. Specifically, we set the G1, S, G2 and M phase to respectively occupy 11/24:ths, 8/24:ths, 4/24:ths and 1/24:th of a cell's individual cell-cycle, in terms of time. These values can be amended upon availability of cell-line specific data. Thus the time spent in each of the four distinct cell-cycles, for a well-oxygenated cell i with a cell-cycle length τ_i, is here $\Theta_{G1}\tau_i$, $\Theta_S\tau_i$, $\Theta_{G2}\tau_i$ and $\Theta_M\tau_i$ for the cell-cycle phases G1, S, G2 and M respectively so that

$$\Theta_{G1}\tau_i + \Theta_S\tau_i + \Theta_{G2}\tau_i + \Theta_M\tau_i = \tau_i. \tag{2}$$

However, low cellular oxygen levels have been shown to delay cell-cycle progression by inducing arrest in particularly the G1 phase of the cell cycle [39]. Mathematically, the cell-cycle can be modelled in various ways. For example, in mechanistic cell-cycle models derived by Tyson and Novak, the cell-cycle is governed by a regulatory molecular network that can be described by a system of ordinary differential equations [40]. By incorporating hypoxia-induced factors in the system of equations, the G1 phase can be inherently elongated under hypoxic conditions [35]. In this study, however, cell-cycle progression is merely modelled using a phenomenological clock, instead of a more detailed Tyson-Novak type of model. As a result of this, there is no mechanistic functionality driving G1-arrest under hypoxic conditions in our model. To remedy

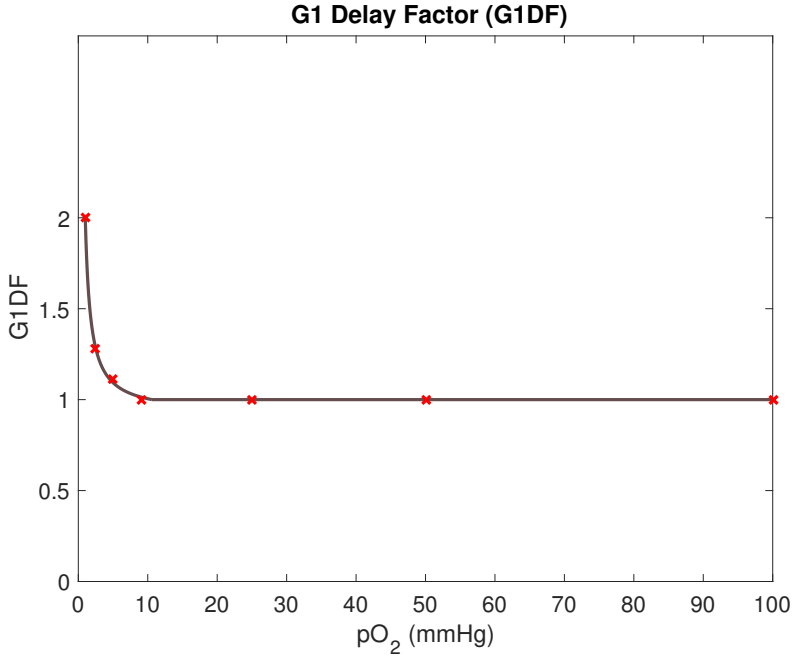

Figure 2: The G1 Delay Factor (G1DF) is incorporated in the model to achieve oxygen-dependent G1 arrest. The G1DF (dark line) is extrapolated from *in vitro* data (red crosses) from a previous mathematical study by Alarcon *et al.* [39].

this fact, we here introduce an additional function to achieve an oxygen-dependent length (in units of time) of the G1-phase. We name this function the G1 Delay Factor ($G1DF$) such that,

$$G1DF(\hat{K}(x,t)) = \begin{cases} a_1 + \frac{a_2}{a_3 + \hat{K}(x,t)} & \text{if } \mathrm{pO}_2 \leq 10.5 \text{ mmHg } (x,t), \\ 1 & \text{otherwise,} \end{cases} \tag{3}$$

where $\hat{K}(x,t)$ denotes the oxygenation (in units of mmHg) of cell in point x at time t. The G1DF, which is illustrated in Figure 2, is an approximation for how much the G1 phase is expanded in time as a function of oxygen pressure, here measured in units of mmHg. The G1DF is matched to fit data points extracted from a previous mathematical study by Alarcon *et al.* [39], in which a Tyson-Novak cell-cycle model is extended to incorporate the action of p27, a protein that is upregulated under hypoxia and delays cell-cycle progression. Thus the time spent in the G_1 phase, τ_{G1}, is given by

$$\tau_{G1} = G1DF(\hat{K}(x,t)) \cdot \Theta_{G1}\tau_i, \tag{4}$$

where $G1DF(\hat{K}(x,t)) = 1$ for normoxic cells ($\hat{K}(x,t) \geq 10$ mmHg). The lengths of other cell-cycle phases are approximated as non-oxygen dependent in the model.

2.3 Tumour Growth

In the model, a tumour is grown from one seeding cancer cell which divides and gives rise to a heterogeneous MCTS. Once a viable, i.e. undamaged, cell has completed the mitosis (M) phase of the cell-cycle, a secondary cell, namely a daughter cell, is produced and placed in the neighbourhood its mother cell. In the model, this cell-division occurs provided that free space is available on the lattice in the νth order neighbourhood of the mother cell, where the value for ν is here fitted form experimental data [34]. This replicates a scenario in which tumour growth may be inhibited by lack of resources such as space or nutrients, as might for example occur *in vitro*. (By setting $\nu = \infty$, the model can be adapted to disregard these cell-division constraints [36]). If this is not the case, no daughter cell is produced, and instead the mother cell assumes a state in which they progress through the cell-cycle very slowly (simulating an *in vitro* spheroid case, in which inner cancer cells experimentally have shown a reduced proliferation rate [34]), or not at all (simulating an *in vivo* case in which cells may enter a quiescent G0 phase [35]). Should neighbourhood space be made available again, as a result of cells getting removed from the lattice due to anticancer treatments, such cells may re-assume an actively cycling state. Each daughter cell is placed on a random lattice point in the neighbourhood of the mother cell, where up to ν spherical neighbourhoods are regarded. In order to agree with the MCTS data [34] used to calibrate the model, we here pick $\nu = 3$, as illustrated in Figure 3, and thus a daughter cell may be placed up to three neighbourhoods away from its mother cell. To accomplish spherical-like tumour growth the model stochastically alternates between deploying Moore and von Neumann neighbourhoods [35]. In the work presented by this paper, neither necrotic nor apoptotic tumour cells are included in the pre-treatment tumour growth model, and instead we make the simplifying modelling assumption that the density of viable cells is constant (one cancer cell per lattice point) within the simulated MCTSs before any treatment is given. However, CA are easily adaptable and, if appropriate and desired, modelling rules concerning necrotic and/or apoptotic cells can be included in the mathematical framework. The *in vitro* experiment produced and reported by Voissiere *et al.* [34] does detect apoptotic cells in the MCTSs, these are primarily located towards the center of the spheroids.

2.4 Oxygen Distribution and Hypoxia

Oxygen is assumed to be readily available in the extracellular matrix and, accordingly, extracellular lattice points are oxygen source points. On the other hand, viable (i.e. non-damaged) cells are modelled as oxygen sinks as they consume oxygen in order to function. The distribution of oxygen across the lattice is modelled by a mechanistic partial differential equation (PDE), specifically a reaction-diffusion equation such that

$$\frac{\partial K(x,t)}{\partial t} = \nabla \cdot (D_K(x,t)\nabla K(x,t)) + r_K m(x,t) - \phi_K K(x,t) cell(x,t), \tag{5}$$

coupled with no-flux boundary conditions. Here $K(x,t)$ denotes the oxygen level in lattice point x at time t. $D_K(x,t)$ is the diffusion coefficient, which is higher in lattice points occupied by cells compared to unoccupied lattice points, so that oxygen diffuses slower over cancer cells than in extracellular material in the model [35]. The binary function $cell(x,t)$ is equal to one if the lattice point is occupied by a cancer cell, and zero otherwise. Similarly, the binary function $m(x,t)$

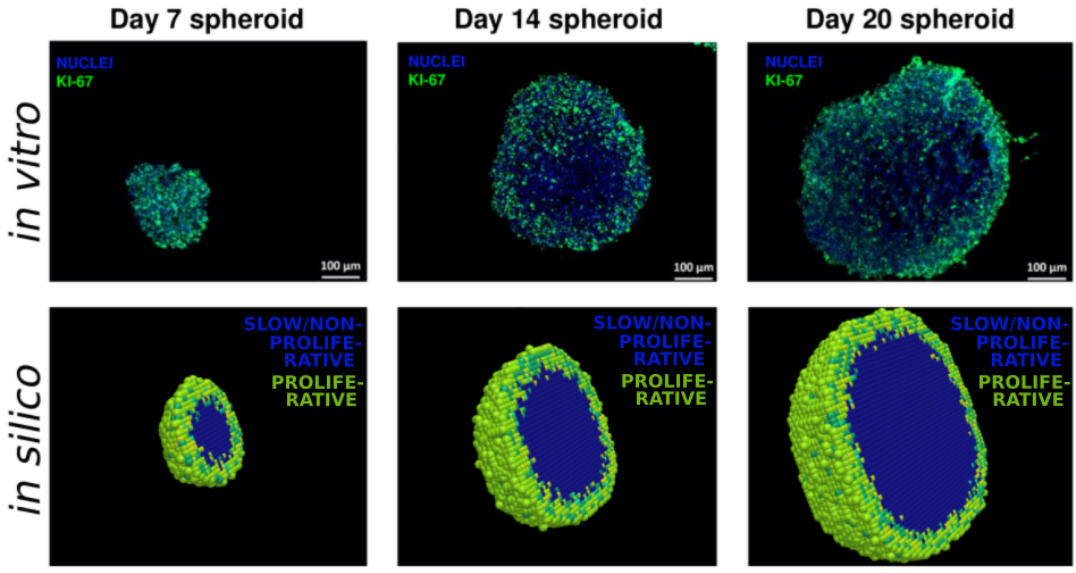

Figure 3: Top: Images from *in vitro* experiments performed by Voissiere *et al.* [34], in which cell nuclei are stained blue and furthermore proliferative cells are stained green by the proliferation marker Ki-67. Bottom: Images from *in silico* experiments performed in this study, where proliferative (cycling) cells are coloured green and inner, slow or non-proliferative cells are coloured blue.

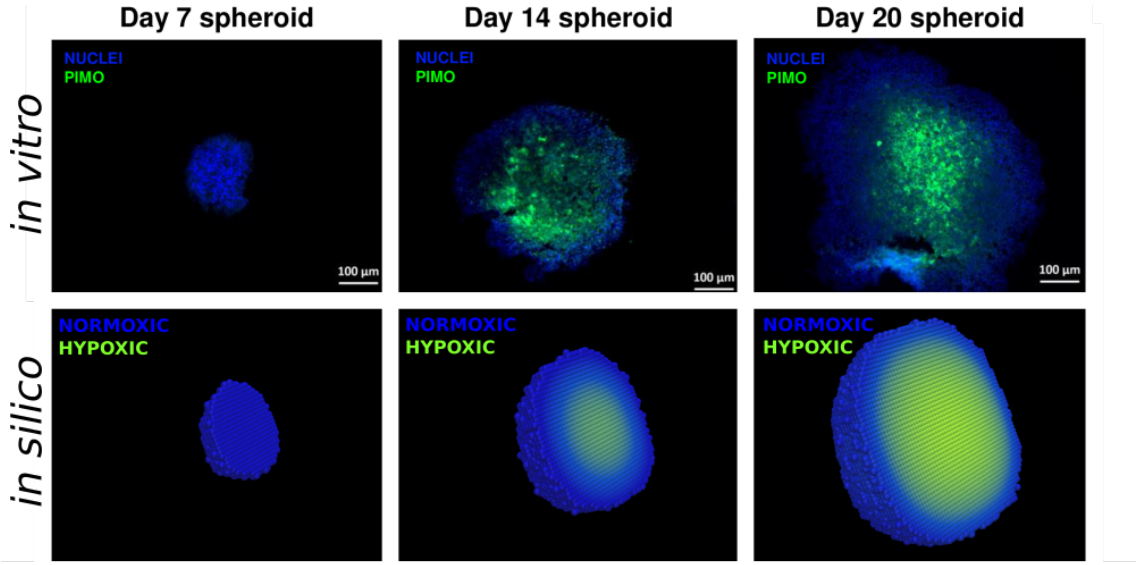

Figure 4: Top: Images from *in vitro* experiments performed by Voissiere *et al.* [34], in which hypoxic cells are stained green by pimonidazole and normoxic cells are stained blue. Bottom: Images from *in silico* experiments performed in this study, where hypoxic cells ($pO_2 \leq 10$ mmHg) are coloured green and normoxic cells ($pO_2 > 10$ mmHg) are coloured blue.

is one if the lattice point is outside the tumour, and zero otherwise. The oxygen production rate is denoted by r_K and the cellular oxygen consumption rate is ϕ_K. Thus the first term in the Equation 5 describes oxygen diffusion, the second term describes oxygen production and the final term describes cellular oxygen consumption. In the model, the diffusion coefficient for oxygen is gathered from literature but the production and consumption rates are calibrated *in silico* to match *in vitro* data from Voissiere *et al.* [34], specifically to achieve appropriate oxygen gradients. Note that the no-flux boundary condition causes the total amount of oxygen on the lattice to increase over time. To express oxygenation levels on the lattice in scaled form, a scaled oxygen variable $\hat{K}(x,t)$ is introduced which is obtained by

$$\hat{K}(x,t) = \frac{K(x,t)}{max_n K(n,t)} \cdot h, \tag{6}$$

where $max_n K(n,t)$ denotes the maximal $K(x,t)$-value (of all n lattice points) at time t [41]. The scaling-factor, h, (with unit mmHg), is incorporated in order to calibrate the model to fit the MCTS data, as illustrated in Figure 4. A cell is defined to be hypoxic if it has a scaled oxygen value such that $\hat{K}(x,t) \leq 10$ mmHg [35]. In the model, the $\hat{K}(x,t)$-value influences G1-arrest (Figure 2), radio-sensitivity (Figure 7) and HAP-AHAP bioreduction rates (Figure 5).

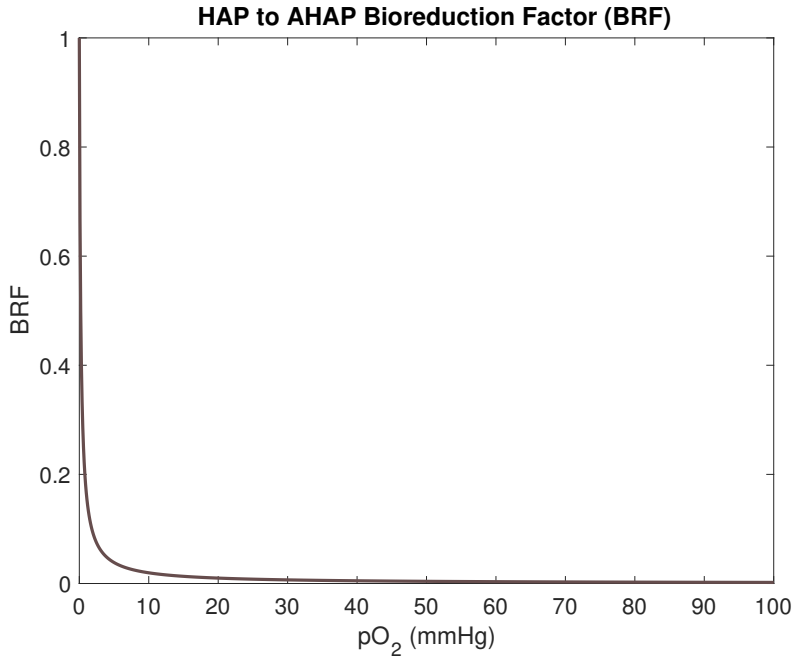

Figure 5: The bioreduction factor, BRF, expresses the fraction of HAP compound that reduces to AHAP compound within one hour as a function of oxygenation (measured in mmHg)

2.5 Hypoxia Activated Prodrugs

Anticancer prodrugs constitute relatively harmless compounds in their inactivated form with the potential to bioreduce, or transform, into cytotoxic species [21]. Specifically for HAPs, this bioreduction occurs in hypoxic conditions and thus HAPs are able to selectively target hypoxic tumour regions [21]. The oxygen dependent bioreduction is here modelled by the function $f_{HAP\to AHAP}(\hat{K}(x,t))$, where

$$f_{HAP\to AHAP}(x,t) = b \cdot BRF(\hat{K}(x,t)), \tag{7}$$

where b is a time-scaling factor with and BRF is a bioreduction factor as illustrated in Figure 5 and

$$BRF(\hat{K}(x,t)) = \frac{[pO_2]_{50}}{[pO_2]_{50} + \hat{K}(x,t)}. \tag{8}$$

Here $[pO_2]_{50}$ denotes the oxygen value yielding 50% bioreduction (in one hour), chosen to be 0.2 mmHg, for evofosfamide, as is done in a previous mathematical model by Hong *et al.* [42]. As illustrated in Figure 5, the BRF value rapidly decreases for pO_2 values (i.e. $\hat{K}(x,t)$ values) between 0 and 10 mmHg.

The mechanistic reaction-diffusion equations governing the distribution of HAPs and AHAPs across the lattice are respectively given by [43]

$$\frac{\partial [HAP](x,t)}{\partial t} = \nabla \cdot (D_{[HAP]}(x,t)\nabla [HAP](x,t)) + r_{[HAP]}(x,t)m(x,t) - f_{HAP\rightarrow AHAP}(x,t)[HAP](x,t) - \eta_{[HAP]}[HAP](x,t), \tag{9}$$

$$\frac{\partial [AHAP](x,t)}{\partial t} = \nabla \cdot (D_{[AHAP]}(x,t)\nabla [AHAP](x,t)) + f_{HAP\rightarrow AHAP}(x,t)[HAP](x,t) - \eta_{[AHAP]}[AHAP](x,t), \tag{10}$$

where $[HAP](x,t)$ denotes the concentration of HAPs and $[AHAP](x,t)$ denotes the concentration of AHAPs in point x at time t. $D_{[HAP]}(x,t)$ and $D_{[AHAP]}(x,t)$ denote the respective diffusion coefficients, $r_{[HAP]}(x,t)$ denotes the HAP production rate, $\eta_{[HAP]}$ and $\eta_{[AHAP]}$ denote the corresponding decay rates. AHAPs are harmful agents which are here assumed to inflict damage that is cell-cycle non-specific. Consequently, cells that are in any cell-cycle phase (G1, S, G2, M), including cells that are in a slow or non-cycling state in the centre of the MCTS, are susceptible to AHAP-inflicted damage in the model. A cell in point x at time t is damaged by the cytotoxic AHAPs if $[AHAP](x,t) \geq \Psi$, where Ψ is the lethal AHAP concentration threshold. Ψ and the production coefficient in Equation 9 are calibrated *in silico* to make it so that HAPs and IR yield the same effect (in terms of number of cells killed) for a large tumour (see the Large Tumour in Figure 8). When a cell dies, it reduces to a membrane-enclosed cell-corpse which is (*in vivo*) digested by macrophages [44]. In the model, the time it takes for a cell to receive lethal damage until it is removed from the lattice, to give space to other cells, is denoted $T_{L\rightarrow R}$ (L for lethal, R for removal). Three cases for this time $T_{L\rightarrow R}$ are investigated in this study: (*i*) the first extreme case in which a dead cell in *never* removed from the lattice (simulating an *in vitro environment*), (*ii*) the other extreme case in which a cell is *instantaneously* removed from the lattice upon receiving lethal damage, and (*iii*) a mid-way case in which a cell is removed from the lattice after a time-period corresponding to its doubling time has passed, i.e. $T_{L\rightarrow R,i} = \tau_i$. Results using the first case are included in the main text, results for cases (*ii*) and (*iii*) are provided in the Supplementary Material in which we demonstrate that, within the scope of the performed *in silico* experiments, this choice of $T_{L\rightarrow R}$ value does not affect our qualitative findings.

2.5.1 Parameters

In our mathematical model, HAPs are produced on the source points (i.e. extracellular lattice points outside the tumour) and are quickly distributed across the lattice. Drug transportation of HAPs from source points to cells is mediated only by the diffusion terms in Equation 9 and and similarly AHAP transportation is mediated only by the diffusion term in Equation 10. Consequently, the drug diffusion coefficients $D_{[HAP]}$ and $D_{[AHAP]}$ represent all biophysical drug transportation across the lattice *in silico*. HAPs must possess certain appropriate

attributes in order to produce desired effects [18]. Specifically, HAPs should be able to travel relatively long distances without being metabolised, specifically distances longer than that of which oxygen travels, in order to reach hypoxic tumour regions. As oxygen is consumed by the cells, whilst HAPs require certain micro-environmental conditions to be met in order to metabolise, HAPs may reach regions located relatively far away from blood vessels, that oxygen can not reach. It has, indeed, been demonstrated *in vivo* that TH-302 has the ability to reach hypoxic regions, where it is activated [45]. Conversely, AHAPs should travel relatively short distances in order to localise AHAP activity to tumour regions only, and thus to minimise unwanted extratumoural toxicity. The diffusion length of oxygen is reported in literature to be approximately 100 μm [35] however, to our knowledge, no diffusion length of neither TH-302 nor Br-IPM has been explicitly reported. However, the diffusion length of the HAP/AHAP pair AQ4N/AQ4 has been shown to be reach roughly 1.5 times that of oxygen (or 150μm) in xenografts [46]. With this motivation, we here approximate the diffusion coefficient of TH-302 to be twice that of oxygen. (*According to the relationship* $L = \sqrt{D/\Phi}$*, where* L *is the diffusion length scale and* Φ *is the compound uptake, the diffusion coefficient of a certain compound,* D*, is proportional to* L^2*, neglecting details of compound uptake [35]. Thus here we make the simplified approximation that* $L_{[HAP]}(x,t) = \sqrt{2} \cdot D_K(x,t)$*.*) Similar to previous procedure, the diffusion length of AHAPs is approximated to be half that of oxygen from which it follows that $D_{[AHAP]}(x,t) = (1/4) \cdot D_K(x,t)$. These parameter estimations suffice to conceptually, and qualitatively, describe the nature of HAPs and AHAPs, but can be amended upon the availability of new data. By adjusting the diffusion coefficients $D_{[HAP]}$ and $D_{[AHAP]}$, the influence of bystander effects are allowed to range from negligible to highly influential in our mathematical framework.

The half-life times of TH-302 and Br-IPM have been reported to be 0.81h and 0.70h respectively in a clinical trial [11], these values are used to determine the decay rates $\eta_{[HAP]}$ and $\eta_{[AHAP]}$. This half-life time of TH-302 is in accordance with preclinical predictions obtained from allometric scaling [26]. Note that the drug decay coefficients, $\eta_{[HAP]}$ and $\eta_{[AHAP]}$ in Equation 9 and Equation 10 respectively, simulate all drug clearance from the system, i.e. both metabolic clearance and excretion.

2.6 Radiotherapy

Cellular responses to radiotherapy are dependent on oxygenation status [4], cell-cycle phase [47, 48], and cell-line characteristics. Cellular radiotherapy responses are here modelled using an appropriate CA adaptation of the widely accepted Linear-Quadratic (LQ) model. In the traditional LQ model, the survival fraction of a cell population is given by $S(d) = e^{-nd(\alpha+\beta d)}$, where d is the radiation dosage, n is the number of administered radiation fractions and α and β are cell-line specific sensitivity parameters [49]. To include cell-cycle sensitivity, α and β are here cell-cycle dependent and the oxygen modification factor (OMF) is incorporated to include oxygen sensitivity [50], such that

$$\mathrm{OMF} = \frac{\mathrm{OER}(\hat{K}(x,t))}{\mathrm{OER}_m} \tag{11}$$

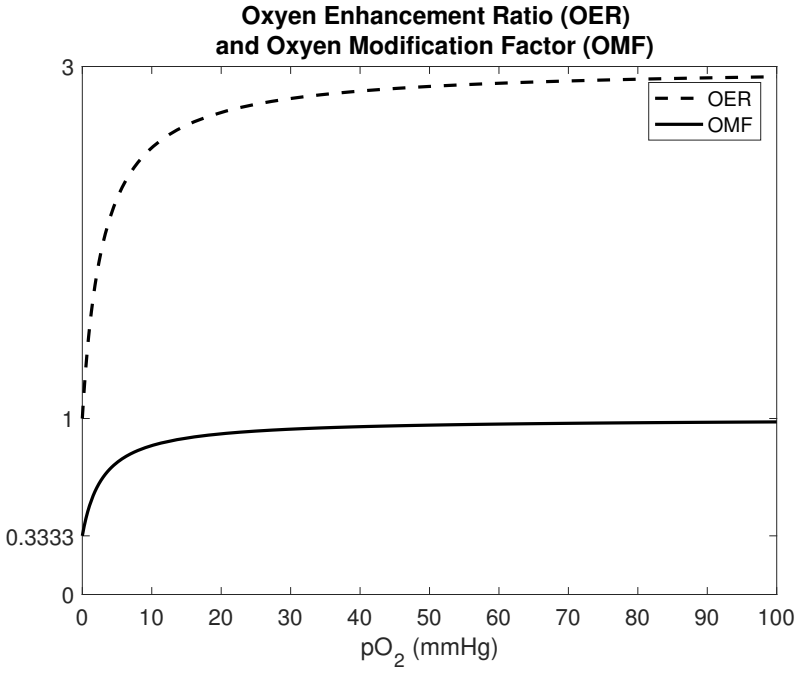

Figure 6: The Oxygen Enhancement Ratio (OER) and the Oxygen Modification Factor (OMF) are incorporated in the mathematical model to quantify the influence of oxygen on radiotherapy responses. Cells are the most least radiosensitive for low pO_2 values. The OER and OMF curves have steep gradients between the oxygen values 0 and 10 mmHg, after which they respectively asymptote to the values 3 and 1 for higher oxygen values.

where

$$\mathrm{OER}(\hat{K}(x,t)) = \frac{\mathrm{OER}_m \cdot \hat{K}(x,t) + K_m}{\hat{K}(x,t) + K_m}, \tag{12}$$

where $\mathrm{OER}_m = 3$ is the maximum value under well-oxygenated conditions and $K_m = 3$ mmHg is the pO_2 value achieving half maximum ratio [41]. The OER and OMF functions are illustrated in Figure 6.

The survival probability of a cell in point x at time t is here given by

$$S(x,t) = e^{-d([OMF]\alpha(x,t)+d[OMF]^2\beta(x,t))}, \tag{13}$$

where the cell-cycle phase specific α and β values are gathered from a previous study by Kempf *et al.* [51], and are listed in Table 1. Cellular responses to a 2Gy IR dose for a generic cancer cell-line, as a function of oxygenation and cell-cycle phase details, are illustrated in Figure 7.

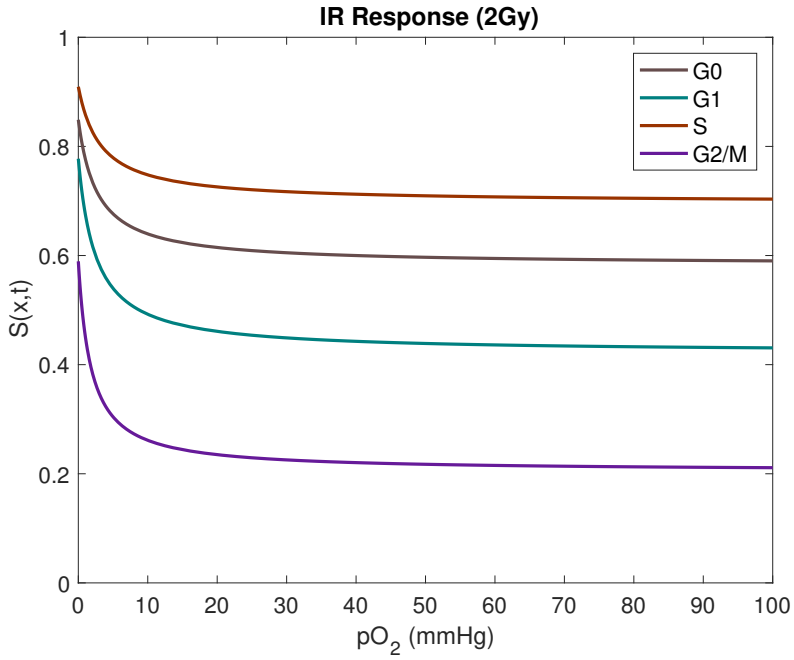

Figure 7: The probability that a cell, in the mathematical model, exposed to a radiotherapy dose of 2 Gy survives. The survival probability $S(x,t)$ is function of its cell-cycle phase and oxygenation value. Cells are the least radiosensitive when hypoxic.

Section, Equation	Parameter	Value
Cellular Automaton		
2.1, N/A	$\Delta x_1 = \Delta x_2 = \Delta x_3$ (spacing)	20 μm
	Δt	0.001 hours
Cell-cycle and proliferation		
2.2, N/A	μ, σ	40 hours, 4 hours
2.2, 1	θ_{G1}, θ_S, θ_{G2}, θ_M	$\frac{11}{24}$, $\frac{8}{24}$, $\frac{4}{24}$, $\frac{1}{24}$
2.2, 4	a_1, a_2, a_3	0.9209, 0.8200, -0.2389
2.3, N/A	ν	3
Oxygen		
2.4, 5	$D_K(x,t) = \begin{cases} D_K/1.5 & \text{if cell in } (x,t) \\ D_K & \text{otherwise} \end{cases}$ $cell(x,t) = \begin{cases} 1 & \text{if cell in } (x,t) \\ 0 & \text{otherwise} \end{cases}$ $m(x,t) = \begin{cases} 1 & \text{if } (x,t) \text{ outside MCTS} \\ 0 & \text{otherwise} \end{cases}$	$D_K = 2.5 \times 10^{-5}$ cm^{2}s^{-1}
2.4, 6	h	0.5 mmHg
2.6, 11	OER_m	3
2.6, 12	K_m	3 mmHg
Drugs		
2.5, 7	b	$(\text{hour})^{-1}$
2.5, 8	$[pO_2]_{50}$	0.2 mmHg
2.5, 9 and 10	D_{HAP}, D_{AHAP}	$2 \times D_K(x,t)$, $\frac{1}{4} \times D_K(x,t)$
	η_{HAP} , η_{AHAP}	*picked from half-life times:* $t_{1/2,HAP}$=0.81 hours, $t_{1/2,AHAP}$=0.70 hours
2.5, 9	$T_{L \to R}$ (for the no removal *in vitro* case)	Infinity
Radiotherapy		
2.6, 13	α(G1), β(G1)	0.351, 0.04
	α(S), β(S)	0.1235, 0.04
	α(G2), β(G2)	0.793, 0
	α(M), β(M)	0.793, 0
	α(G0), β(G0)	α(G1)/1.5, β(G1)/(1.5^2)

Table 1: A summary of model parameters used in the mathematical framework.

2.7 Parameters

In this study we attempt to replicate the nature of generic eukaryotic cell-lines, the HAP evofosfamide (TH-302) and its corresponding AHAP, Br-IPM. The parameters, which are listed in Table 1, are chosen accordingly but can be adapted to represent other specific cell-lines or drugs upon data becoming readily available.

2.8 Implementation and *in silico* Framework

The mathematical model is implemented in an in-house computational framework written in C++ deploying high-performance computing techniques. The PDEs describing oxygen and drug distribution across the lattice are solved using explicit finite difference methods with no-flux boundary conditions. Maps of cancer cells and the microenvironment are visualised in

ParaView [52]. Using this computational framework, various experimental *in vitro* and *in vivo* scenarios are formulated and simulated *in silico*. In order to grow an *in silico* MCTS, one seeding cancer cell is placed on the lattice and this cell divides and gives rise to a MCTS that is heterogeneous in nature, as in-built model stochasticity creates cell-cycle asyncronosity amongst tumour cells [53], and oxygen levels vary across the MCTS. Such virtual spheroids are thereafter subjected to various treatment combinations comprising HAPs and IR. Treatment commence when MCTSs consist of, in the order of, 100,000 cancer cells or 'agents' in our agent-based model. Due to the high number of agents, and the fact that the intrinsic model stochasticity only involves a few events during the simulated treatment time (specifically 0-3 cell divisions and potentially one response to radiotherapy) the quantitative results do not differ much between *in silico* runs. Performing the same *in silico* experiment 10 times yields a standard deviation that can be regarded as negligible (less than 0.5%), and thus we argue that basing our results from means from 10 simulation runs per experiment is enough to mitigate intrinsic model stochasticity to a level that is sufficient for this qualitative study.

3 Results and Discussion

In Sections 3.1 through to 3.3, we compare treatment responses in two different *in silico* tumour spheroids, specifically a 'Large' and more hypoxic MCTS and a 'Small', less hypoxic MCTS. The 'Small' tumour corresponds to the 20 day-old MCTS in Figures 3 and 4, that is calibrated by *in vitro* data from Voissiere *et al.* [34]. The 'Large' MCTS is extrapolated by letting the 'Small' MCTS grow for yet another 10 days *in silico*, until it reaches an age of 30 days. The 'Small' and 'Large' MCTSs are illustrated in Figure 8.

The simulated IR dose is chosen to be 2 Gy, and to allow for intuitive comparisons between the two different monotherapies, the HAP dose (Dose_{HAP}) is here qualitatively chosen, and calibrated to yield the a similar *in silico* response as the 2 Gy IR dose (in terms of cell survival) in the 'Large' MCTS. Quantitative doses can be specified and implemented upon the availability of data.

3.1 HAP and IR monotherapies attack tumours in different ways

In this initial *in silico* experiment, a MCTS is subjected to a monotherapy of either one dose of HAPs or one dose of IR. Our *in silico* results demonstrate that HAP and IR monotherapies attack the MCTS in different ways. This can be understood by regarding the treatment responses in Figure 9 and Figure 10. Figure 9 shows cell-cycle phase specific survival data, in terms of cell count over time, when the 'Small' or 'Large' MCTS is subjected to a HAP or IR monotherapy. Similarly, Figure 10 shows the composition of cells, in terms of their cell-cycle phase, in response to a HAP or IR monotherapy dose. Our results demonstrate that for the 'Small', well-oxygenated MCTS, HAPs have negligible effect on the cell count (see Figure 9) and, by extension, on the cell-cycle phase composition (see Figure 10). This shows that, by design, HAP treatments have little effect on tumours that are not hypoxic enough to cause significant HAP-to-AHAP bioreduction. For the 'Large' MCTS, however, HAPs successfully eliminate cells, particularly the inner cells of the MCTS, labeled 'Slow/non-proliferative' (see

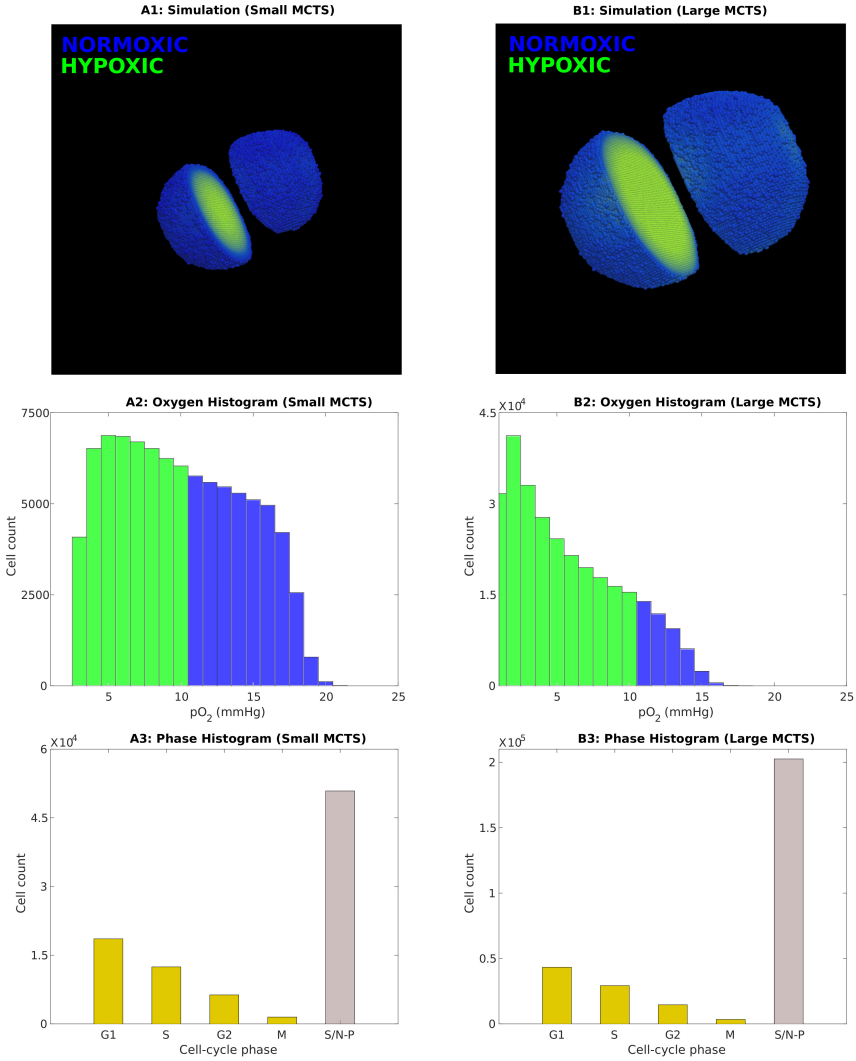

Figure 8: The 'Small' (20 day old) MCTS and the 'Large' (30 day old) MCTS are used in Sections 3.1, 3.2, 3.3 to allow for comparisons in treatment responses between tumours with different oxygenation levels. Top: Simulation snapshots of the MCTSs at the time point T_0 when treatments commence (A1: Small MCTS, B1: Large MCTS). Hypoxic cells ($pO_2 \leq 10$ mmHg) are green whilst normoxic cells are blue. Middle: Oxygen histograms at time T_0, in which hypoxic cell counts are shown in green and normoxic cell counts are shown in blue (A2: Small MCTS, B2: Large MCTS). Bottom: Cell-cycle phase histograms at time T_0 (A3: Small MCTS, B3: Large MCTS). The slow/non-proliferative, inner cancer cells are labeled S/N-P.

Figure 9). This causes an alteration in the cell-cycle phase composition in favour of the proliferative cells in the outer shell of the MCTS (see Figure 10). Our results further show that, for both the 'Small' and the 'Large' MCTSs, IR eliminates cells of all cell-cycle states (see Figure 9), but alters the cell-cycle phase composition in favour of the inner, hypoxic cells as these are

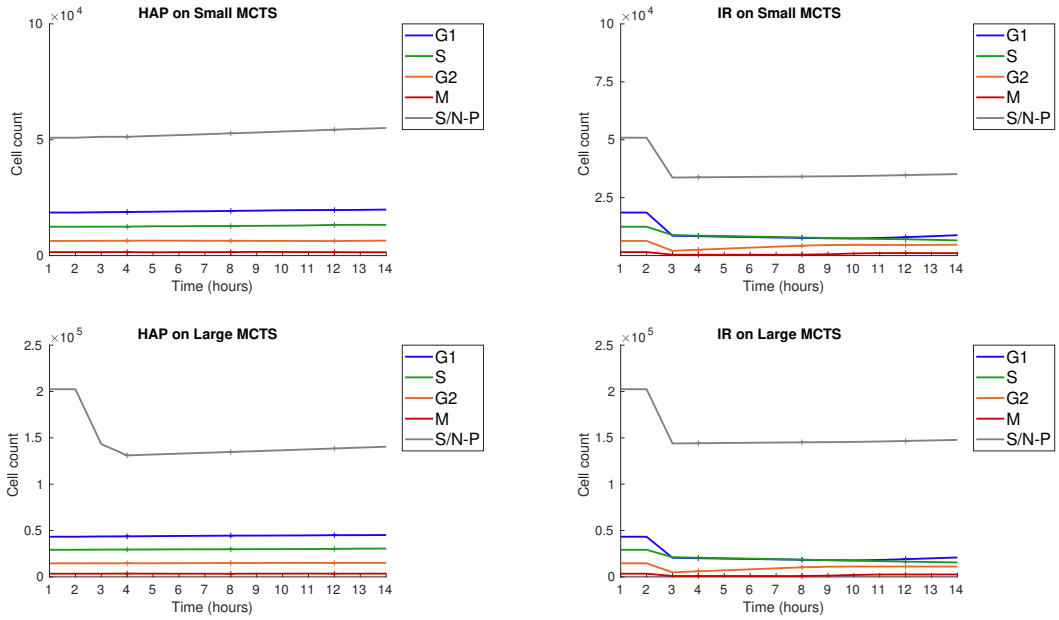

Figure 9: Treatment responses for HAPs (left) and IR (right) monotherapies for the 'Small' (top) and 'Large' (bottom) MCTS. The monotherapy is given at 0 hours. Graphs demonstrate cell-cycle specific cell count (i.e. number of viable, undamaged cells) over time. The slow/non-proliferative, inner cancer cells are labeled S/N-P. Solid lines show mean values, and '+' markers show standard deviations for 10 *in silico* runs.

less sensitive to radiotherapy (see Figure 10). These opposing effects on the cell-cycle phase composition achieved by HAPs and IR in the 'Large' MCTS indicate that, for tumours that are hypoxic enough for HAPs to have an effect, HAP-IR combination treatments have the potential of producing multifaceted attacks on tumours.

Since radiation responses are enhanced by the presence of molecular oxygen, we investigated which monotherapy (i.e. HAP or IR) best eliminates hypoxic cells and reoxygenates MCTSs after one single treatment dose. To demonstrate the overall alteration of oxygenation levels in the MCTSs as a result of the monotherapies, Figure 11 provides histograms for cellular oxygenation levels at time T_0 (the time of therapy administration) and at time $T_0 + 4$ hours. From this figure we can see that for the 'Small' MCTS, HAPs do not alter the overall intra-tumoural oxygenation but IR does, since HAPs are not efferctive but IR is. For the 'Large' MCTS, on the other hand, both HAPs and IR alter the overall intra-tumoural oxygenation but only HAPs manage to eliminate the most hypoxic cells, and thus shift the oxygen histogram away from the most severe levels of hypoxia. This indicates that administering HAPs as a neoadjuvant therapy prior to radiotherapy may enhance the effect of radiotherapy in tumours that are sufficiently hypoxic for HAPs to be effective.

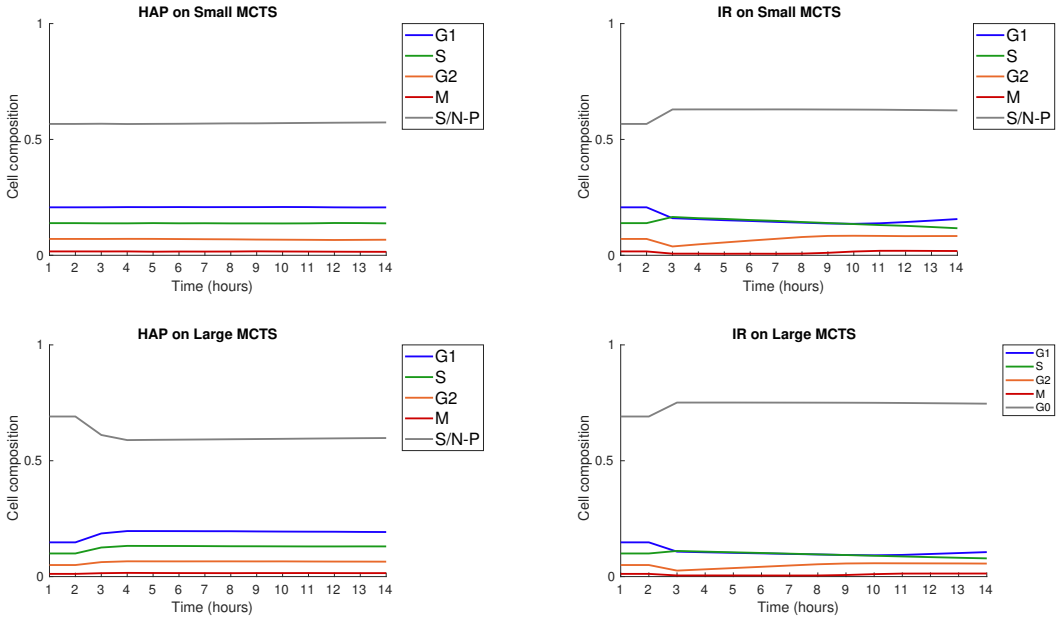

Figure 10: Treatment responses for HAPs (left) and IR (right) monotherapies for the 'Small' (top) and 'Large' (bottom) MCTS. The monotherapy is given at 0 hours. Graphs demonstrate cell-cycle specific composition (of viable, undamaged cells) over time. The slow/non-proliferative, inner cancer cells are labeled S/N-P. Solid lines show mean values for 10 *in silico* runs (standard deviations are negligible hence not shown).

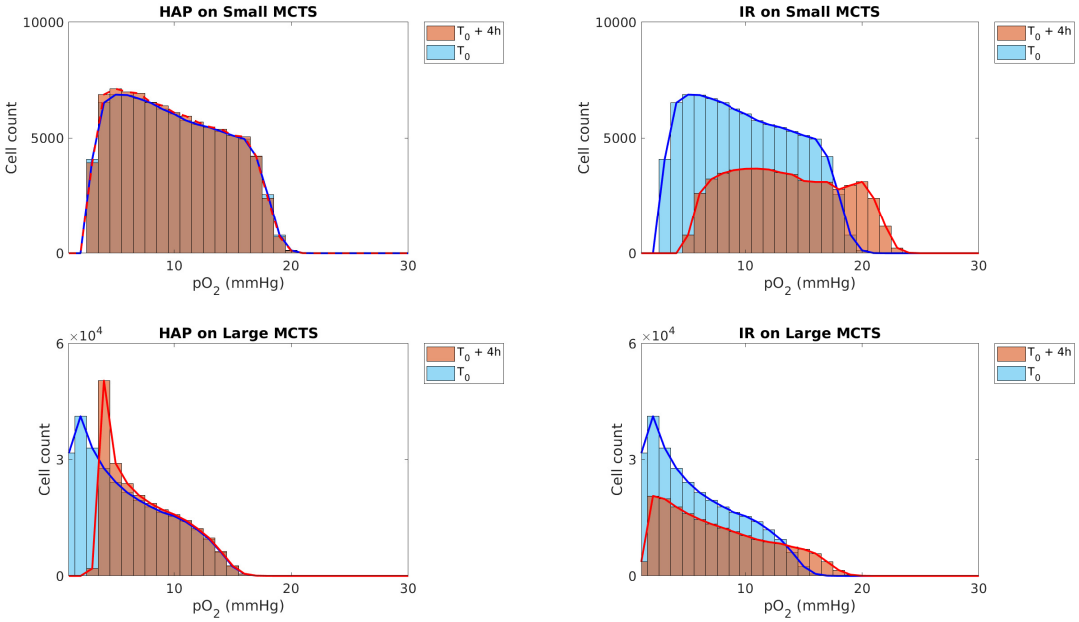

Figure 11: Treatment responses for HAPs (left) and IR (right) monotherapies for the 'Small' (top) and 'Large' (bottom) MCTS. Histograms over cellular oxygenation levels at time T_0 (monotherappy administration time) and 4 hours later are shown. Results are based on mean values from 10 *in silico* runs.

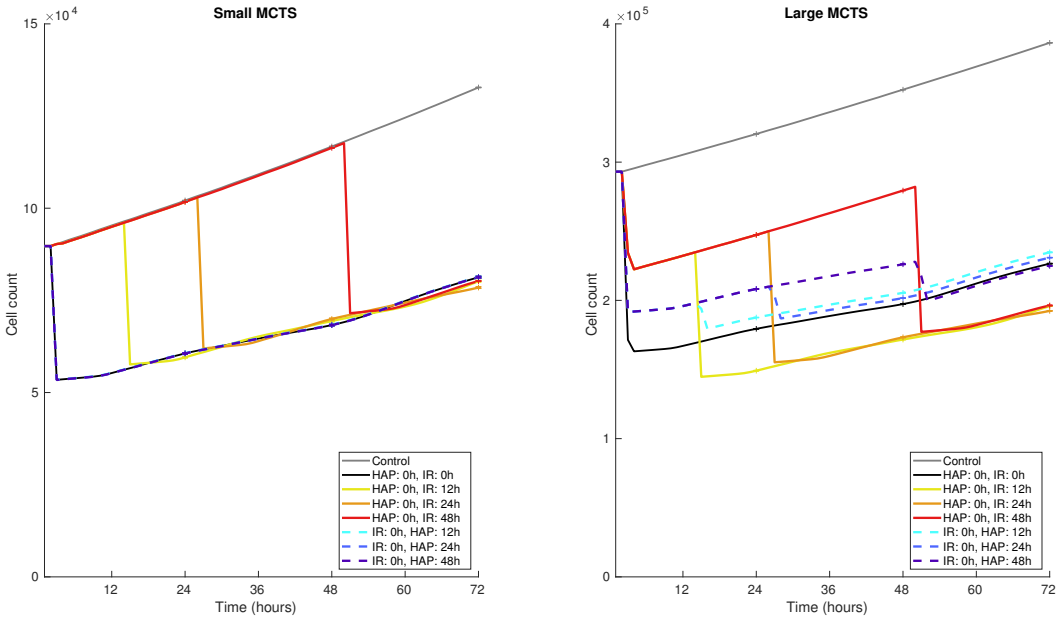

Figure 12: Treatment responses (in terms of cell count) for HAP-IR combination therapies in the 'Small' MCTS (left) and the 'Large' MCTS (right). One dose of HAPs and one dose of IR are administered at various schedules. Solid and dashed lines show mean values, and '+' markers show standard deviations for 10 *in silico* runs.

3.2 HAP-IR treatment scheduling impacts HAP efficacy in sufficiently hypoxic tumours

In order to study the optimal treatment scheduling of HAP-IR combination therapies, simulated MCTSs are here given one dose of HAPs and one dose of IR, using different schedules. Figure 12 shows the cell count over time when one dose of HAPs and one dose of IR are administered with various schedules. Specifically, either HAPs is given at 0 hours (followed by IR at 0, 12, 24 or 48 hours) or IR is given at 0 hours (followed by HAPs at 0, 12, 24 or 48 hours). The results in Figure 12 demonstrate that for the 'Small' MCTS, scheduling does not impact the overall treatment outcome, as HAPs are not effective. For the 'Large' MCTS however, it is more effective to give HAPs before IR, than to give IR before HAPs. This indicates that, in tumours that are hypoxic enough for HAPs to be effective, the HAP-IR treatment scheduling impacts the efficacy of the combination treatment.

3.3 HAPs enhance radiotherapy effects in sufficiently hypoxic tumours

To investigate if and when HAPs enhance the effect of radiotherapy, simulated MCTSs are subjected to either IR monotherapies or HAP-IR combination therapies. In the combination therapy case, HAPs are administered at time T_0 and IR is administered at time $T_0 + 48$ hours. In the

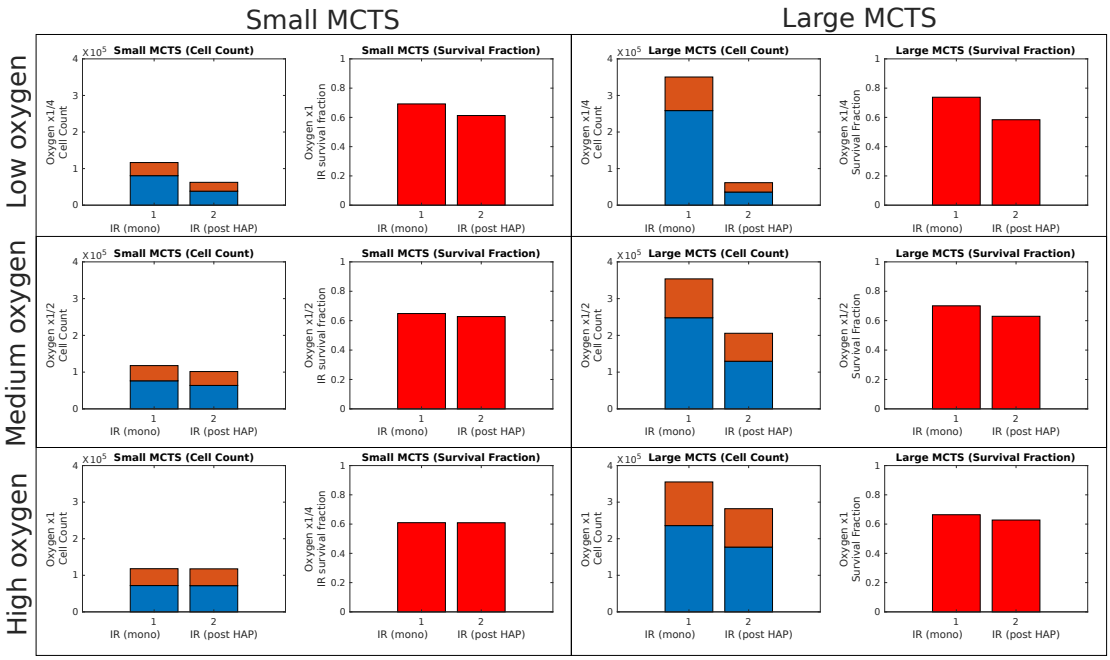

Figure 13: Treatment responses of radiotherapy in various MCTSs when either (1) an IR monotherapy dose is administered at T_0+48 hours or (2) IR is given at T_0+48 hours following a prior HAP dose at time T_0. Note that only explicit IR responses (not HAP responses) are shown. The oxygen-levels of the 'Small' (left) and 'Large' (right) tumours are scaled by a factor of 1 (least hypoxic), 1/2 or 1/4 (most hypoxic). The value calibrated from *in vitro* experiments [34] correspond to the scaling with factor 1. Orange + blue bars show number of viable cells (instantaneously) before IR administration, blue bars show the number of viable cells (instantaneously) post IR. Red bars show how many cells (as a fraction) survived the IR attack.

monotherapy case, radiotherapy is administered at time $T_0 + 48$ hours. For a thorough investigation, the oxygen-levels of the 'Large' and 'Small' tumours are further scaled by multiplication with a factor 1, 1/2 or 1/4 so that we have 6 different tumours on which to test if neoadjuvant HAPs enhances radiotherapy efficacy. Figure 13 shows IR treatment responses in form of survival data (both in terms of number of surviving cells and fraction of surviving cells). From these plots we see that for very hypoxic MCTSs, the administration of neoadjuvant HAPs does increase the effect of radiotherapy. However, for well-oxygenated MCTS, neoadjuvant HAPs do not increase the effect of radiotherapy.

3.4 The intratumoural oxygen landscape impacts HAP efficacy

In Sections 3.1, 3.2, 3.3 we have demonstrated various ways that the intra-tumoural oxygenation level impacts HAP and IR monotherapies and combination therapies. Further, in order to investigate if the spatio-temporal intumoural oxygen landscape impacts HAP efficacy, two

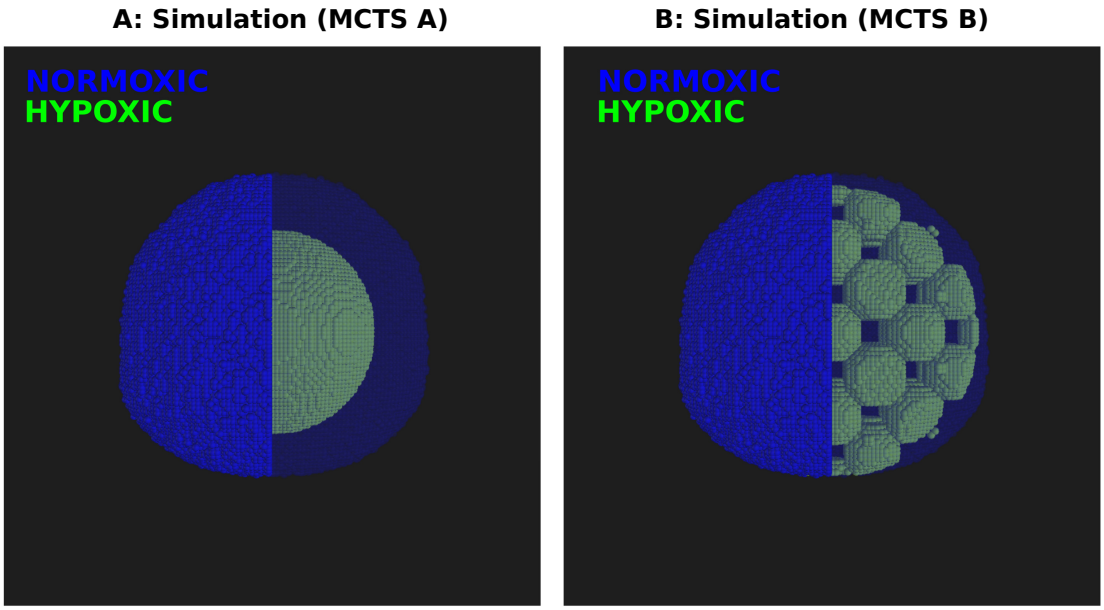

Figure 14: MCTS A and B prior to treatment commencing. The MCTSs are visualised in both opaque and transparent formats. Hypoxic activator cells are shown in green and normoxic bystander cells counts are shown in blue. Activator and bystander cells are manually set so that MCTSs A and B contain the same number of activator and bystander cells.

MCTSs with different oxygen landscapes are here compared. Omitting details of oxygen dynamics and vessel structure, hypoxic regions are here manually assigned in the MCTSs so that every cancer cell is set to be either severely hypoxic ($p_O2 = 0$ mmHg) or very well-oxygenated ($p_O2 = 100$ mmHg). Both MCTSs, named MCTS A and MCTS B, are assigned the same number of severely hypoxic and well-oxygenated cancer cells at the time-point when treatment commences. In MCTS A, the hypoxic region is made up of one concentric sphere in the core of the MCTS, whilst in MCTS B, the hypoxic regions consist of multiple spheres, evenly spread out across the MCTS. MCTS A and MCTS B are illustrated in Figure 14. The severely hypoxic cancer cells are here called *activator cells*, as the prodrug bioreduction (or activation) is maximal in severly hypoxic environments. The well-oxygenated cells are here referred to as *bystander cells*, as the bioreduction is minimal in well-oxygenated environments. Thus any lethal AHAP concentration occurring in a bystander cell is a result of HAP-to-AHAP bioreduction occurring outside the bystander cells.

From Figure 15 it is clear that the bystander effects are higher in MCTS B than in MCTS A, although all activator cells are eliminated in both MCTSs. When the activator cells are spread out across the spheroid, as in MCTS B, there are more interfaces in which bystander cells experience significant bystander effects. Although the oxygen landscape in MCTS B is highly synthetic, this *in silico* experiment shows that the intratumoural oxygen landscape impacts the efficacy of HAPs.

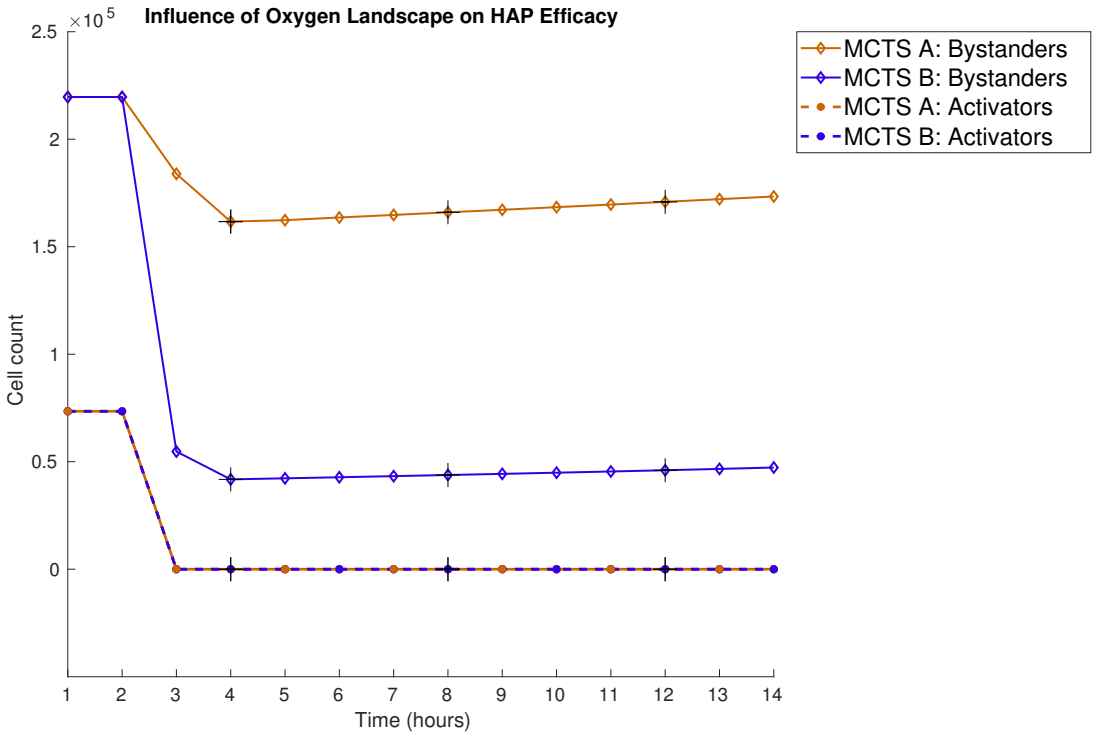

Figure 15: Treatment responses in MCTS A and MCTS B when HAPs are administered at 0 hours. The number of viable (undamaged) cells are plotted over time for MCTS A and MCTS B tumour. Activator cells ($pO_2 = 0$ mmHg) are shown in dashed lines and bystander ($pO_2 = 100$ mmHg) cells shown in solid lines. Results show mean values for 10 *in silico* runs and '+' markers show standard deviations.

4 Conclusion

Previous *in vitro* and *in vivo* studies have validated the successfulness of HAPs in laboratory settings, however, this preclinical success has not yet been reflected in clinical trials. In an attempt to elucidate the unsatisfactory results from clinical HAP trials, we in this study investigate how oxygen-related tumour features and treatment administration plans impact the efficacy of HAP monotherapies and HAP-IR combination therapies *in silico*. To this end we have developed a mathematical model capturing the spatio-temporal dynamics of tumours subjected to multimodality treatments comprising HAPs and IR. A set of results (*i* to *iv*) relating to HAP efficacy *in silico* have here been demonstrated.

i HAPs and IR attack tumours in different, complementary, fashions. Whilst IR provides a highly effective way to kill cancer cells in tumours, hypoxic and resting cells are significantly more resistant to IR than are well-oxygenated and actively cycling cells. HAPs, however, are alkylating agents which bioreduce in (primarily) hypoxic areas, hence HAPs primarily inflict damage in hypoxic tumour regions, which are especially susceptible to HAP damage. Consequently, HAP-IR combination treatments have the potential of produce a multifaceted attack on tumours.

ii In sufficiently hypoxic tumours, the HAP-IR treatment schedule influences treatment efficacy. However, in well oxygenated tumours the schedule is not important.

iii In sufficiently hypoxic tumours, HAP functions as a treatment intensifier, however, in well oxygenated tumours it does not.

iv Not only the overall intra-tumoural oxygenation levels, but also the intratumoural oxygen landscape, impacts HAP efficacy.

In a recent publication, Spiegelberg *et al.* [1], claim that the (lack of) clinical progress with HAP-treatments can, in great part, be attributed to the omission of hypoxia-based patient selection. This *in silico* demonstrates that whilst HAPs are effective treatment intensifiers for sufficiently hypoxic tumours, they have negligible effect on more well-oxygenated tumours. In simple terms: some tumours are suitable to be paired with treatment plans involving HAPs whilst others are not. In line with Spiegelberg *et al.*'s claims [1], our *in silico* results indicate that a personalised medicine approach is preferable if treatments involving HAPs (that are similar to TH-302) are to achieve their maximum potential in clinical settings. In this study, we qualitatively studies various aspects of HAP-IR treatment schedules using a multiscale mathematical framework. Upon the availability of *in vitro* and *in vivo* data, this mathematical framework can be calibrated in order to serve as an *in silico* testbed for predicting HAP-IR treatment scenarios. As a result of interdisciplinary collaborations, the mathematical framework used in this study has previously been validated *in vitro* and *in vivo* for applications other than HAP-IR combination treatments [54, 36]. The multiscale nature of the framework enables integration of data from various scales, be it from the subcellular scale, the cellular scale or the tissue scale. As an example of useful data, the multi cellular tumour spheroid data previously produced by Voissiere *et al.* [34] provided our framework with calibration data for tumour growth and spatio-temporal

oxygen dynamics. Using existing experimental data to create data-driven mathematical models is a resourceful step involved in the advancement of mathematical oncology [55].

Acknowledgements

SH was supported by the Medical Research Council [grant code MR/R017506/1] and Swansea University PhD Research Studentship. LJD, AY and PL acknowledge financial support from ERC advanced grant (ERC-ADG-2015, n° 694812 Hypoximmuno) and EUROSTARS (COMPACT 12053).

5 Supplementary Material

5.1 Complement to Figure 12

Figures 16 and 17 show that the Scheduling-Experiment, performed in Section 3.2 and with results provided in Figure 12, are qualitatively the same if a damaged cell is instantly removed from the lattice (Figure 16) or if a damaged cell is moved from the lattice after a time period corresponding to its doubling time (Figure 17).

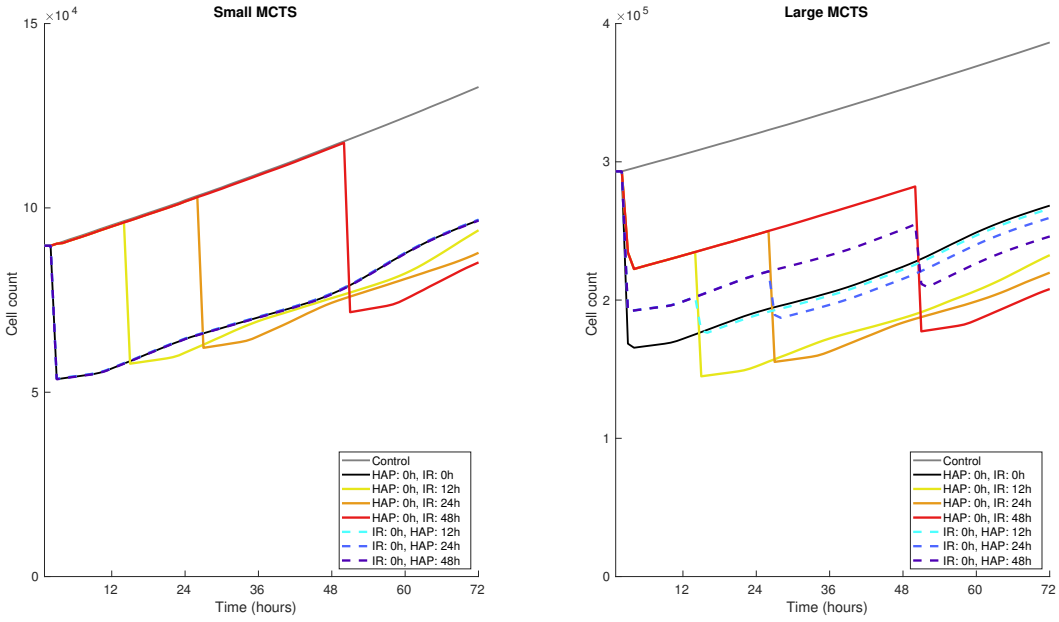

Figure 16: Scheduling of HAP-IR combination treatments, Complement to Figure 12. Cells are removed from the lattice instantaneously after the lethal event occurred.

5.2 Complement to Figure 13

Figures 18 and 19 show that the experiment that investigates if HAPs act as radiotherapy enhancers, discussed in Section 3.3 and with results provided in Figure 13, are qualitatively the same if a damaged cell is instantly removed from the lattice (Figure 18) or if a damaged cell is moved from the lattice after a time period corresponding to its doubling time (Figure 19).

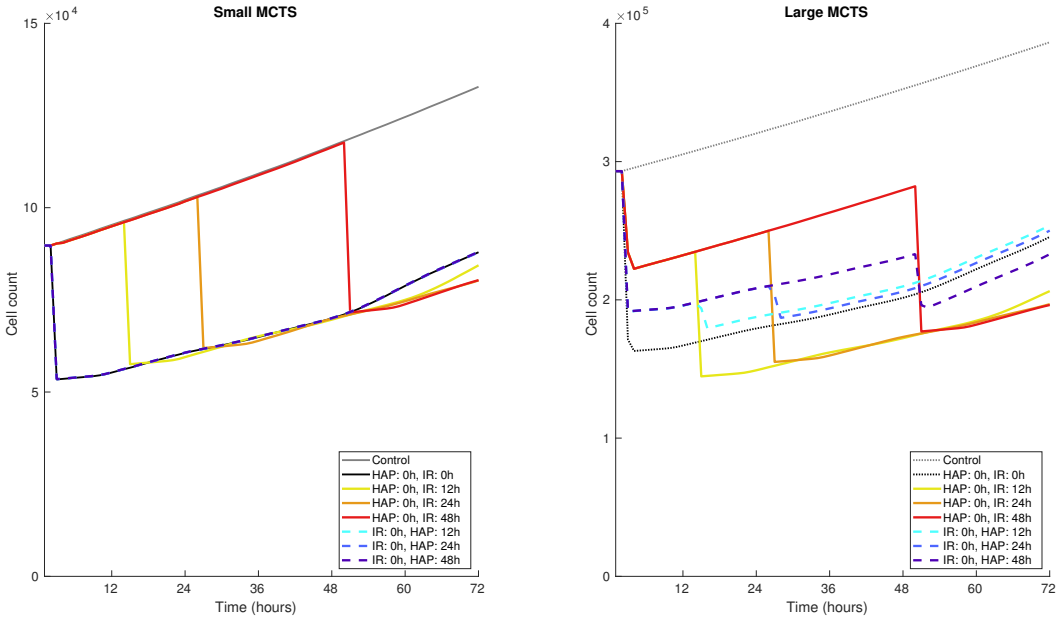

Figure 17: Scheduling of HAP-IR combination treatments, Complement to Figure 12. Cells are removed from the lattice after a time corresponding to their doubling time (τ_i) post the lethal event occurred.

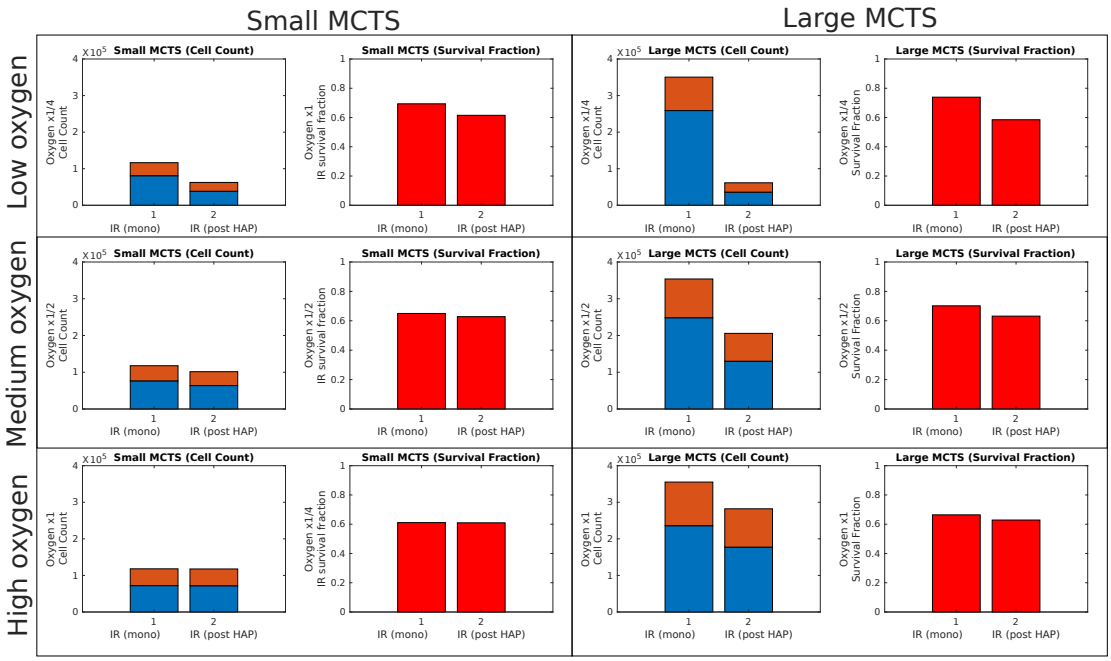

Figure 18: Treatment responses of radiotherapy in various MCTSs when either (1) an IR monotherapy dose is administered at T_0+48 hours or (2) IR is given at T_0+48 hours following a prior HAP dose at time T_0. Complement to Figure 13. Cells are removed from the lattice instantaneously after the lethal event occurred.

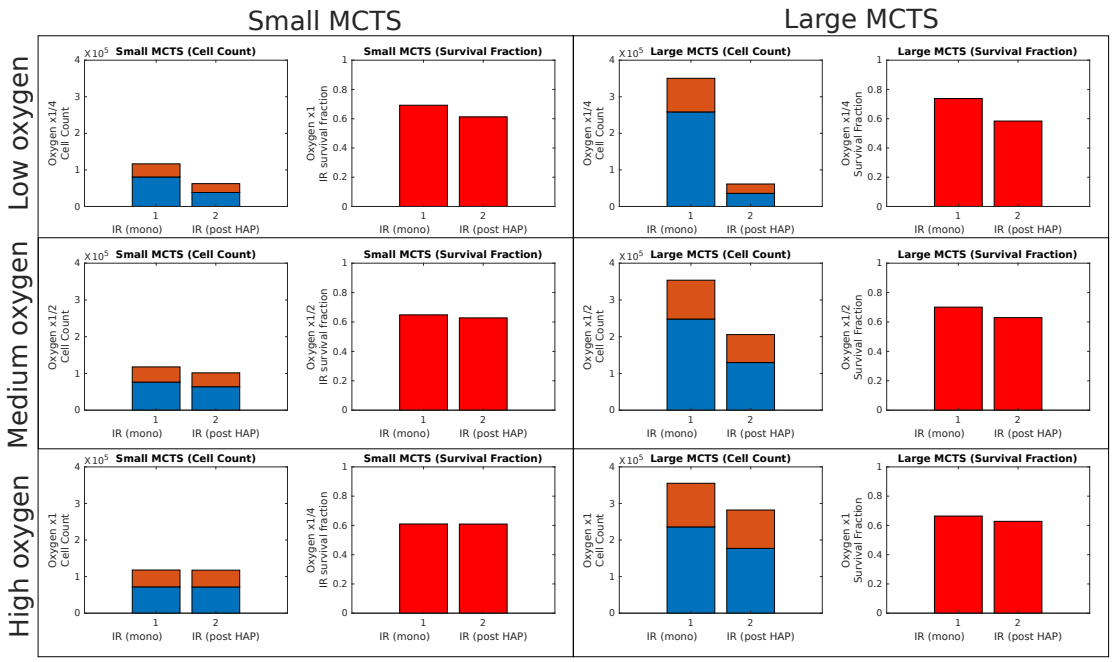

Figure 19: Treatment responses of radiotherapy in various MCTSs when either (1) an IR monotherapy dose is administered at T_0+48 hours or (2) IR is given at T_0+48 hours following a prior HAP dose at time T_0. Complement to Figure 13. Cells are removed from the lattice after a time corresponding to their doubling time (τ_i) post the lethal event occurred.

References

[1] L. Spiegelberg, R. Houben, R. Niemans, D. de Ruysscher, A. Yaromina, J. Theys, C. P. Guise, J. B. Smaill, A. V. Patterson, P. Lambin, and L. J. Dubois, "Hypoxia-activated prodrugs and (lack of) clinical progress: The need for hypoxia-based biomarker patient selection in phase III clinical trials," *Clin Transl Radiat Oncol* **15** (Feb, 2019) 62–69.

[2] F. W. Hunter, B. G. Wouters, and W. R. Wilson, "Hypoxia-activated prodrugs: paths forward in the era of personalised medicine," *Br. J. Cancer* **114** no. 10, (May, 2016) 1071–1077.

[3] W. A. Denny, "Hypoxia-activated prodrugs in cancer therapy: progress to the clinic," *Future Oncol* **6** no. 3, (Mar, 2010) 419–428.

[4] M. R. Horsman and J. Overgaard, "The impact of hypoxia and its modification of the outcome of radiotherapy," *J. Radiat. Res.* **57 Suppl 1** (Aug, 2016) i90–i98.

[5] C. T. Lee, M. K. Boss, and M. W. Dewhirst, "Imaging tumor hypoxia to advance radiation oncology," *Antioxid. Redox Signal.* **21** no. 2, (Jul, 2014) 313–337.

[6] V. Liapis, A. Labrinidis, I. Zinonos, S. Hay, V. Ponomarev, V. Panagopoulos, M. DeNichilo, W. Ingman, G. J. Atkins, D. M. Findlay, A. C. Zannettino, and A. Evdokiou, "Hypoxia-activated pro-drug TH-302 exhibits potent tumor suppressive activity and cooperates with chemotherapy against osteosarcoma," *Cancer Lett.* **357** no. 1, (Feb, 2015) 160–169.

[7] Q. Liu, J. D. Sun, J. Wang, D. Ahluwalia, A. F. Baker, L. D. Cranmer, D. Ferraro, Y. Wang, J. X. Duan, W. S. Ammons, J. G. Curd, M. D. Matteucci, and C. P. Hart, "TH-302, a hypoxia-activated prodrug with broad in vivo preclinical combination therapy efficacy: optimization of dosing regimens and schedules," *Cancer Chemother. Pharmacol.* **69** no. 6, (Jun, 2012) 1487–1498.

[8] I. N. Mistry, M. Thomas, E. D. D. Calder, S. J. Conway, and E. M. Hammond, "Clinical Advances of Hypoxia-Activated Prodrugs in Combination With Radiation Therapy," *Int. J. Radiat. Oncol. Biol. Phys.* **98** no. 5, (08, 2017) 1183–1196.

[9] S. G. Peeters, C. M. Zegers, R. Biemans, N. G. Lieuwes, R. G. van Stiphout, A. Yaromina, J. D. Sun, C. P. Hart, A. D. Windhorst, W. van Elmpt, L. J. Dubois, and P. Lambin, "TH-302 in Combination with Radiotherapy Enhances the Therapeutic Outcome and Is Associated with Pretreatment [18F]HX4 Hypoxia PET Imaging," *Clin. Cancer Res.* **21** no. 13, (Jul, 2015) 2984–2992.

[10] J. D. Sun, Q. Liu, J. Wang, D. Ahluwalia, D. Ferraro, Y. Wang, J. X. Duan, W. S. Ammons, J. G. Curd, M. D. Matteucci, and C. P. Hart, "Selective tumor hypoxia targeting by hypoxia-activated prodrug TH-302 inhibits tumor growth in preclinical models of cancer," *Clin. Cancer Res.* **18** no. 3, (Feb, 2012) 758–770.

[11] G. J. Weiss, J. R. Infante, E. G. Chiorean, M. J. Borad, J. C. Bendell, J. R. Molina, R. Tibes, R. K. Ramanathan, K. Lewandowski, S. F. Jones, M. E. Lacouture, V. K. Langmuir, H. Lee, S. Kroll, and H. A. Burris, "Phase 1 study of the safety, tolerability, and pharmacokinetics of TH-302, a hypoxia-activated prodrug, in patients with advanced solid malignancies," *Clin. Cancer Res.* **17** no. 9, (May, 2011) 2997–3004.

[12] N. Baran and M. Konopleva, "Molecular Pathways: Hypoxia-Activated Prodrugs in Cancer Therapy," *Clin. Cancer Res.* **23** no. 10, (May, 2017) 2382–2390.

[13] J. Hu, D. R. Handisides, E. Van Valckenborgh, H. De Raeve, E. Menu, I. Vande Broek, Q. Liu, J. D. Sun, B. Van Camp, C. P. Hart, and K. Vanderkerken, "Targeting the multiple myeloma hypoxic niche with TH-302, a hypoxia-activated prodrug," *Blood* **116** no. 9, (Sep, 2010) 1524–1527.

[14] C. P. Guise, A. M. Mowday, A. Ashoorzadeh, R. Yuan, W. H. Lin, D. H. Wu, J. B. Smaill, A. V. Patterson, and K. Ding, "Bioreductive prodrugs as cancer therapeutics: targeting tumor hypoxia," *Chin J Cancer* **33** no. 2, (Feb, 2014) 80–86.

[15] W. A. Denny, "The role of hypoxia-activated prodrugs in cancer therapy," *Lancet Oncol.* **1** no. 1, (Sep, 2000) 25–29.

[16] W.-L. Liao, S.-C. Lin, H. S. Sun, and S.-J. Tsai, "Hypoxia-induced tumor malignancy and drug resistance: Role of micrornas," *Biomarkers and Genomic Medicine* **6** no. 1, (2014) 1 – 11.

[17] J. X. Duan, H. Jiao, J. Kaizerman, T. Stanton, J. W. Evans, L. Lan, G. Lorente, M. Banica, D. Jung, J. Wang, H. Ma, X. Li, Z. Yang, R. M. Hoffman, W. S. Ammons, C. P. Hart, and M. Matteucci, "Potent and highly selective hypoxia-activated achiral phosphoramidate mustards as anticancer drugs," *J. Med. Chem.* **51** no. 8, (Apr, 2008) 2412–2420.

[18] F. Meng, J. W. Evans, D. Bhupathi, M. Banica, L. Lan, G. Lorente, J. X. Duan, X. Cai, A. M. Mowday, C. P. Guise, A. Maroz, R. F. Anderson, A. V. Patterson, G. C. Stachelek, P. M. Glazer, M. D. Matteucci, and C. P. Hart, " ," *Mol. Cancer Ther.* **11** no. 3, (Mar, 2012) 740–751.

[19] R. M. Phillips, "Targeting the hypoxic fraction of tumours using hypoxia-activated prodrugs," *Cancer Chemother. Pharmacol.* **77** no. 3, (Mar, 2016) 441–457.

[20] J. Maddison, S. Page, and D. Church, "Small Animal Clinical Pharmacology," . (2008) .

[21] J. D. Sun, Q. Liu, D. Ahluwalia, D. J. Ferraro, Y. Wang, D. Jung, M. D. Matteucci, and C. P. Hart, "Comparison of hypoxia-activated prodrug evofosfamide (TH-302) and ifosfamide in preclinical non-small cell lung cancer models," *Cancer Biol. Ther.* **17** no. 4, (Apr, 2016) 371–380.

[22] C. R. Hong, B. D. Dickson, J. K. Jaiswal, F. B. Pruijn, F. W. Hunter, M. P. Hay, K. O. Hicks, and W. R. Wilson, "Cellular pharmacology of evofosfamide (TH-302): A critical re-evaluation of its bystander effects," *Biochem. Pharmacol.* **156** (10, 2018) 265–280.

[23] A. Foehrenbacher, T. W. Secomb, W. R. Wilson, and K. O. Hicks, "Design of optimized hypoxia-activated prodrugs using pharmacokinetic/pharmacodynamic modeling," *Front Oncol* **3** (Dec, 2013) 314.

[24] Y. Huang, Y. Tian, Y. Zhao, C. Xue, J. Zhan, L. Liu, X. He, and L. Zhang, "Efficacy of the hypoxia-activated prodrug evofosfamide (TH-302) in nasopharyngeal carcinoma in vitro and in vivo," *Cancer Commun (Lond)* **38** no. 1, (May, 2018) 15.

[25] D. Jung, H. Jiao, J. X. Duan, M. Matteucci, and R. Wang, "Metabolism, pharmacokinetics and excretion of a novel hypoxia activated cytotoxic prodrug, TH-302, in rats," *Xenobiotica* **42** no. 4, (Apr, 2012) 372–388.

[26] D. Jung, L. Lin, H. Jiao, X. Cai, J. X. Duan, and M. Matteucci, "Pharmacokinetics of TH-302: a hypoxically activated prodrug of bromo-isophosphoramide mustard in mice, rats, dogs and monkeys," *Cancer Chemother. Pharmacol.* **69** no. 3, (Mar, 2012) 643–654.

[27] K. J. Nytko, I. Grgic, S. Bender, J. Ott, M. Guckenberger, O. Riesterer, and M. Pruschy, "The hypoxia-activated prodrug evofosfamide in combination with multiple regimens of radiotherapy," *Oncotarget* **8** no. 14, (Apr, 2017) 23702–23712.

[28] A. Yaromina, M. Granzier, R. Biemans, N. Lieuwes, W. van Elmpt, G. Shakirin, L. Dubois, and P. Lambin, "A novel concept for tumour targeting with radiation: Inverse dose-painting or targeting the "Low Drug Uptake Volume"," *Radiother Oncol* **124** no. 3, (09, 2017) 513–520.

[29] L. Spiegelberg, S. J. van Hoof, R. Biemans, N. G. Lieuwes, D. Marcus, R. Niemans, J. Theys, A. Yaromina, P. Lambin, F. Verhaegen, and L. J. Dubois, "Evofosfamide sensitizes esophageal carcinomas to radiation without increasing normal tissue toxicity," *Radiother Oncol* (Aug, 2019) .

[30] A. Foehrenbacher, K. Patel, M. R. Abbattista, C. P. Guise, T. W. Secomb, W. R. Wilson, and K. O. Hicks, "The Role of Bystander Effects in the Antitumor Activity of the Hypoxia-Activated Prodrug PR-104," *Front Oncol* **3** (2013) 263.

[31] D. Lindsay, C. M. Garvey, S. M. Mumenthaler, and J. Foo, "Leveraging Hypoxia-Activated Prodrugs to Prevent Drug Resistance in Solid Tumors," *PLoS Comput. Biol.* **12** no. 8, (Aug, 2016) e1005077.

[32] J. W. Wojtkowiak, H. C. Cornnell, S. Matsumoto, K. Saito, Y. Takakusagi, P. Dutta, M. Kim, X. Zhang, R. Leos, K. M. Bailey, G. Martinez, M. C. Lloyd, C. Weber, J. B. Mitchell, R. M. Lynch, A. F. Baker, R. A. Gatenby, K. A. Rejniak, C. Hart, M. C. Krishna, and R. J. Gillies, "Pyruvate sensitizes pancreatic tumors to hypoxia-activated prodrug TH-302," *Cancer Metab* **3** no. 1, (2015) 2.

[33] S. Hamis, G. G. Powathil, and M. A. J. Chaplain, "Blackboard to Bedside: A Mathematical Modeling Bottom-Up Approach Toward Personalized Cancer Treatments," *JCO Clin Cancer Inform* **3** (02, 2019) 1–11.

[34] A. Voissiere, E. Jouberton, E. Maubert, F. Degoul, C. Peyrode, J. M. Chezal, and E. Miot-Noirault, "Development and characterization of a human three-dimensional chondrosarcoma culture for in vitro drug testing," *PLoS ONE* **12** no. 7, (2017) e0181340.

[35] G. G. Powathil, K. E. Gordon, L. A. Hill, and M. A. Chaplain, "Modelling the effects of cell-cycle heterogeneity on the response of a solid tumour to chemotherapy: biological insights from a hybrid multiscale cellular automaton model," *J. Theor. Biol.* **308** (Sep, 2012) 1–19.

[36] S. Hamis, J. Yates, M. Chaplain, and G. Powathil, "Targeting cellular dna damage responses: Predicting in vivo treatment responses using an in vitro-calibrated agent-based mathematical model," *Preprint: bioRxiv, doi: 10.1101/841270* .

[37] S. Hamis, P. Nithiarasu, and G. G. Powathil, "What does not kill a tumour may make it stronger: In silico insights into chemotherapeutic drug resistance," *J. Theor. Biol.* **454** (Jun, 2018) 253–267.

[38] G. Cooper and R. Hausman, "The Cell-A Molecular Approach 4th edition,".

[39] T. Alarcon, H. M. Byrne, and P. K. Maini, "A mathematical model of the effects of hypoxia on the cell-cycle of normal and cancer cells," *J. Theor. Biol.* **229** no. 3, (Aug, 2004) 395–411.

[40] J. J. Tyson and B. Novak, "Regulation of the eukaryotic cell cycle: molecular antagonism, hysteresis, and irreversible transitions," *J. Theor. Biol.* **210** no. 2, (May, 2001) 249–263.

[41] G. Powathil, M. Kohandel, M. Milosevic, and S. Sivaloganathan, "Modeling the spatial distribution of chronic tumor hypoxia: implications for experimental and clinical studies," *Comput Math Methods Med* **2012** (2012) 410602.

[42] C. R. Hong, W. R. Wilson, and K. O. Hicks, "An Intratumor Pharmacokinetic/Pharmacodynamic Model for the Hypoxia-Activated Prodrug Evofosfamide (TH-302): Monotherapy Activity is Not Dependent on a Bystander Effect," *Neoplasia* **21** no. 2, (02, 2019) 159–171.

[43] C. Meaney, G. Powathil, A. Yaromina, L. Dubois, P. Lambin, and M. Kohandel, "Role of hypoxia-activated prodrugs in combination with radiation therapy: An in silico approach," *Mathematical Biosciences and Engineering* **16** (01, 2019) 6257–6273.

[44] H. P. Rang and M. M. Dale, "Rang and dale's pharmacology," *Edinburgh: Elsevier/Churchill Livingstone.* (2012) .

[45] C. Hajj, J. Russell, C. P. Hart, K. A. Goodman, M. A. Lowery, A. Haimovitz-Friedman, J. O. Deasy, and J. L. Humm, "A Combination of Radiation and the Hypoxia-Activated Prodrug Evofosfamide (TH-302) is Efficacious against a Human Orthotopic Pancreatic Tumor Model," *Transl Oncol* **10** no. 5, (Oct, 2017) 760–765.

[46] O. Tredan, A. B. Garbens, A. S. Lalani, and I. F. Tannock, "The hypoxia-activated ProDrug AQ4N penetrates deeply in tumor tissues and complements the limited distribution of mitoxantrone," *Cancer Res.* **69** no. 3, (Feb, 2009) 940–947.

[47] T. M. Pawlik and K. Keyomarsi, "Role of cell cycle in mediating sensitivity to radiotherapy," *Int. J. Radiat. Oncol. Biol. Phys.* **59** no. 4, (Jul, 2004) 928–942.

[48] W. K. Sinclair and W. K. Sinclair, "Cyclic X-ray responses in mammalian cells in vitro. 1968," *Radiat. Res.* **178** no. 2, (Aug, 2012) V112–124.

[49] H. Enderling, M. A. Chaplain, and P. Hahnfeldt, "Quantitative modeling of tumor dynamics and radiotherapy," *Acta Biotheor.* **58** no. 4, (Dec, 2010) 341–353.

[50] G. G. Powathil, M. Swat, and M. A. Chaplain, "Systems oncology: towards patient-specific treatment regimes informed by multiscale mathematical modelling," *Semin. Cancer Biol.* **30** (Feb, 2015) 13–20.

[51] H. Kempf, H. Hatzikirou, M. Bleicher, and M. Meyer-Hermann, "In silico analysis of cell cycle synchronisation effects in radiotherapy of tumour spheroids," *PLoS Comput. Biol.* **9** no. 11, (2013) e1003295.

[52] Ayachit and Utkarsh, "The ParaView Guide: A Parallel Visualization Application, ISBN: 978-1930934306," *Kitware* (2015) .

[53] S. Hamis, S. Stratiev, and G. G. Powathil, "Uncertainty and sensitivity analyses methods for agent-based mathematical models: An introductory review," *(Preprint) arXiv:1911.08429* (2019) .

[54] S. Bruningk, G. Powathil, P. Ziegenhein, J. Ijaz, I. Rivens, S. Nill, M. Chaplain, U. Oelfke, and G. Ter Haar, "Combining radiation with hyperthermia: a multiscale model informed byin vitroexperiments," *J R Soc Interface* **15** no. 138, (Jan, 2018) .

[55] O. Wolkenhauer, C. Auffray, O. Brass, J. Clairambault, A. Deutsch, D. Drasdo, F. Gervasio, L. Preziosi, P. Maini, A. Marciniak-Czochra, C. Kossow, L. Kuepfer, K. Rateitschak, I. Ramis-Conde, B. Ribba, A. Schuppert, R. Smallwood, G. Stamatakos, F. Winter, and H. Byrne, "Enabling multiscale modeling in systems medicine," *Genome Med* **6** no. 3, (2014) 21.